

14. SITE 938¹

Shipboard Scientific Party²

HOLE 938A

Date occupied: 29 April 1994
Date departed: 30 April 1994
Time on hole: 1 day, 4 hr, 45 min
Position: 4°39.504'N, 47°18.740'W
Bottom felt (drill pipe measurement from rig floor, m): 2815.4
Distance between rig floor and sea level (m): 11.26
Water depth (drill pipe measurement from sea level, m): 2804.1
Penetration (m): 310.20
Number of cores (including cores having no recovery): 34
Total length of cored section (m): 310.20
Total core recovered (m): 242.42
Core recovery (%): 78
Oldest sediment cored:
Depth (mbsf): 310.20
Nature: Silty clay
Earliest age: Pleistocene

HOLE 938B

Date occupied: 30 April 1994
Date departed: 1 May 1994
Time on hole: 12 hr, 30 min
Position: 4°39.505'N, 47°18.746'W
Bottom felt (drill pipe measurement from rig floor, m): 2815.3
Distance between rig floor and sea level (m): 11.17
Water depth (drill pipe measurement from sea level, m): 2804.1
Penetration (m): 81.30
Number of cores (including cores having no recovery): 9
Total length of cored section (m): 81.26
Total core recovered (m): 79.53
Core recovery (%): 97
Oldest sediment cored:
Depth (mbsf): 81.30
Nature: Silty clay
Earliest age: Pleistocene

Principal results: Site 938 (proposed Site AF-16) is located on the eastern part of the Amazon Fan, on the flank of the western levee of the abandoned Blue Channel-levee System. The site was intended to provide a hemipelagic biostratigraphic and magnetostratigraphic reference section above the Blue channel-levee System and to sample the Blue levee. Below the Blue levee, we hoped to sample hemipelagic sediment above the levee sediment of Channel 6, which could be compared with Site 932.

The site was selected from a *Farnella* seismic-reflection profile (FR815; 0904 hr on 21 Jan.). A short seismic section and a 3.5-kHz profile across the site were obtained from the pre-site survey from *JOIDES Resolution*.

Hole 938A was cored by APC to 83.6 mbsf, then by XCB to 309.2 mbsf and PCS to 310.2, with total hole recovery of 242.68 m (78.2%). The PCS recovered no sample. Hole 938B was cored to 81.3 mbsf and recovered 79.53 m (97.9%).

Temperature measurements were made at 46 and 84 mbsf (ADARA) and show a mean geothermal gradient of 34°C/km. There was gas expansion in many cores. Methane was found throughout the hole, but higher hydrocarbons were not detected.

Two lithologic units are recognized:

Unit I (0–0.44 mbsf) is a bioturbated, Holocene foraminifer-nannofossil clay, with 33% carbonate at 0.08 mbsf, similar to Unit I at other Leg 155 sites.

Unit II (0.44–306.35 mbsf) consists of mud with intervals of interbedded laminae and beds of silt and very fine sand. The carbonate content of the mud is generally 1%–5%. The unit is subdivided into six subunits on the basis of frequency of silt and sand layers. Subunit IIA (0.44–10.55 mbsf) comprises bioturbated mud. Subunit IIB (10.55–71.84 mbsf) is composed of mud with silt laminae and rare thin beds of silt and very fine sand. Subunit IIC (71.84–117.45 mbsf) consists of mud with numerous silt laminae and beds of silt and very fine sand. Burrow mottles are common and disrupt many silt laminae. Sand beds are as thick as 9 cm. The lower parts of Subunit IIB and Subunit IIC correspond to the flank of the Blue levee. Subunit IID (117.45–170.53 mbsf) is mud with rare silt laminae and common burrow mottling. Carbonate content averages 3.6% and reaches 18.9% in a 2-cm-thick light-colored interval that may be a clast. A few loosely cemented diagenetic nodules of siderite were observed. This subunit corresponds to the seismostratigraphic interval from Channel 5 to the Yellow Channel-levee System. Subunit IIE (170.53–233.73 mbsf) consists of mud with abundant laminae and thin beds of silt and very fine sand. Recovery was only 50% in this interval, suggesting that more sand may have been present than was recovered. Subunit IIE is correlated acoustically with part of the Channel 5 Channel-levee System that appears to have filled abandoned Channel 6. Subunit IIF (233.73–306.35 mbsf) is mud with laminae and thin beds of silt and very fine sand, but in less abundance than in Subunit IIE. The average carbonate content exceeds 3%, compared with <2.5% in the overlying subunit. Subunit IIF corresponds to the upper part of the 200-m-thick Channel 6 levee crest. Changes in the trend of the water-content downhole profile correspond approximately to the upper boundaries of Subunits IID and IIF, suggesting changes in sedimentation rate.

Foraminifer abundances are generally high in Unit I, moderate in Subunits IIA, part of IIC, and IID, and low elsewhere. At 149 mbsf, abundant *P. obliquiloculata* reappears, suggesting an age >40 ka. The absence of *G. menardii* and *G. tumida* at the base of the hole indicates an age <85 ka.

¹Flood, R.D., Piper, D.J.W., Klaus, A., et al., 1995. *Proc. ODP, Init. Repts.*, 155: College Station, TX (Ocean Drilling Program).

²Shipboard Scientific Party is as given in the list of participants in the contents.

Abyssal benthic foraminifers are found in finer grained intervals of Subunits IIB and IIC, suggesting periods of lower sedimentation rate. Bathyal benthic foraminifers in Subunits IID and IIE are associated with iron-stained foraminifers, wood, and mica, and indicate a reworked component.

An apparent paleomagnetic excursion was tentatively identified at 147 mbsf within an XCB core. This event has a similar character to the Lake Mungo Excursion (30 ka) that was identified at a similar seismostratigraphic level at Sites 930 and 933. A clear secular variation pattern was detected in the declination records at two intervals in Hole 938A. Between 15 and 45 mbsf, five cycles are present that can be correlated with cycles of similar character in Holes 937B and 930C. Another sixteen cycles of declination were found between 70 and 78 mbsf in Hole 938A.

The proportion of illite (and mica) to other clay minerals is highest in the interval from 20 to 40 mbsf, corresponding to hemipelagic sediment equivalent to the Amazon, Aqua, and Purple seismostratigraphic intervals. A similar pattern is seen at Site 936 over the same seismostratigraphic units, but at that site the sediment is of levee facies. This suggests that the trend reflects changes in the mineralogy of sediment supplied to the fan, rather than being a consequence of analyzing samples of different grain sizes.

This site has yielded a long biostratigraphic record, and ^{14}C and foraminifer isotopic dating can be related directly to magnetostratigraphy. As at other sites, we have learned that levees are built of irregular alternations of mud-rich and silt-rich intervals, on a scale of a few meters to tens of meters. The good stratigraphic control at this site will help permit an interpretation of such changes.

SETTING AND OBJECTIVES

Introduction

Site 938 (proposed Site AF-16), located on the eastern portion of the Amazon Fan, was intended to provide a hemipelagic reference section in relatively shallow water (2804 m) above the crest of the Blue System, to sample the Blue System, the flat-lying layers separating this levee system from the Channel 6 System below, and the crest of Channel 6. This was the only site during Leg 155 at which the Blue System was sampled. The Channel 6B levee was sampled at Site 932 in deeper water. Channel 6B is linked to Channel 6 up-fan and this site provided the opportunity to sample the same system in shallower water.

Setting

Site 938 is located on the western (left) flank of the Blue System near the shallowest depth to which it can be traced as a bathymetric feature (see Fig. 1, "Site 937" chapter, this volume; Damuth et al., 1988; Manley and Flood, 1988). Cores recovered at Site 932 suggested that Channel 6B is older than 40 ka (it predates the *P. obliquiloculata* datum), and thus we expected to recover a biostratigraphic record about 40,000 years long at this site, with much higher accumulation rates in the Blue levee. This site, Site 937 (proposed Site AF-17), and Site 939 (proposed Site AF-12) are the shallowest-water sites to be drilled during Leg 155.

The site was selected from a *Farnella* seismic profile (FR815; 0904 hr on 12 Jan. 1982). Our pre-site 3.5-kHz and water-gun survey verified the reflection sequence, and the site was chosen at 1243UTC 27 April 1994 on our *JOIDES Resolution* profile (Fig. 1). This appears to be equivalent to the position selected on the *Farnella* line. The site is on the flank of the levee, and thus we expected the record of planktonic material to be more diluted by terrigenous material than at Site 937 (Fig. 2).

The surficial sediment at the site, interpreted from sub-bottom and seismic profiles, includes a drape of acoustically stratified sediment more than 30 ms thick overlying the Blue levee. Parallel reflections

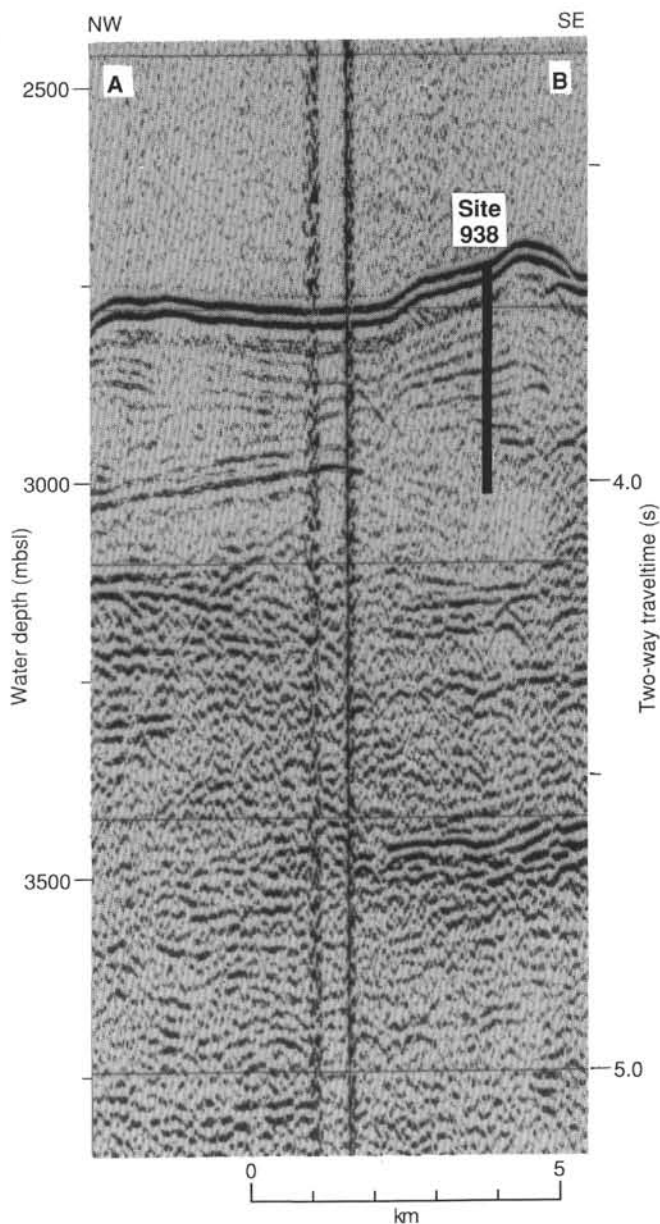


Figure 1. Seismic section through Site 938 (*JOIDES Resolution*). Section is located as A-B on Figure 1 of the "Site 937" chapter, this volume.

mark the base of the Blue levee, and strong reflections are observed in the channel of the underlying Channel 6 levee. The hole ends in levee sediment of Channel 6.

Objectives

The principal objectives at Site 938 were:

1. To sample the anticipated hemipelagic stratigraphic section above the Blue levee on the eastern side of the fan, to determine past changes in ocean circulation, and to aid in developing a fan stratigraphy.
2. To characterize the record of organic matter in a high-sedimentation rate site.
3. To sample the sediment of the Blue System to determine their composition and characteristics.

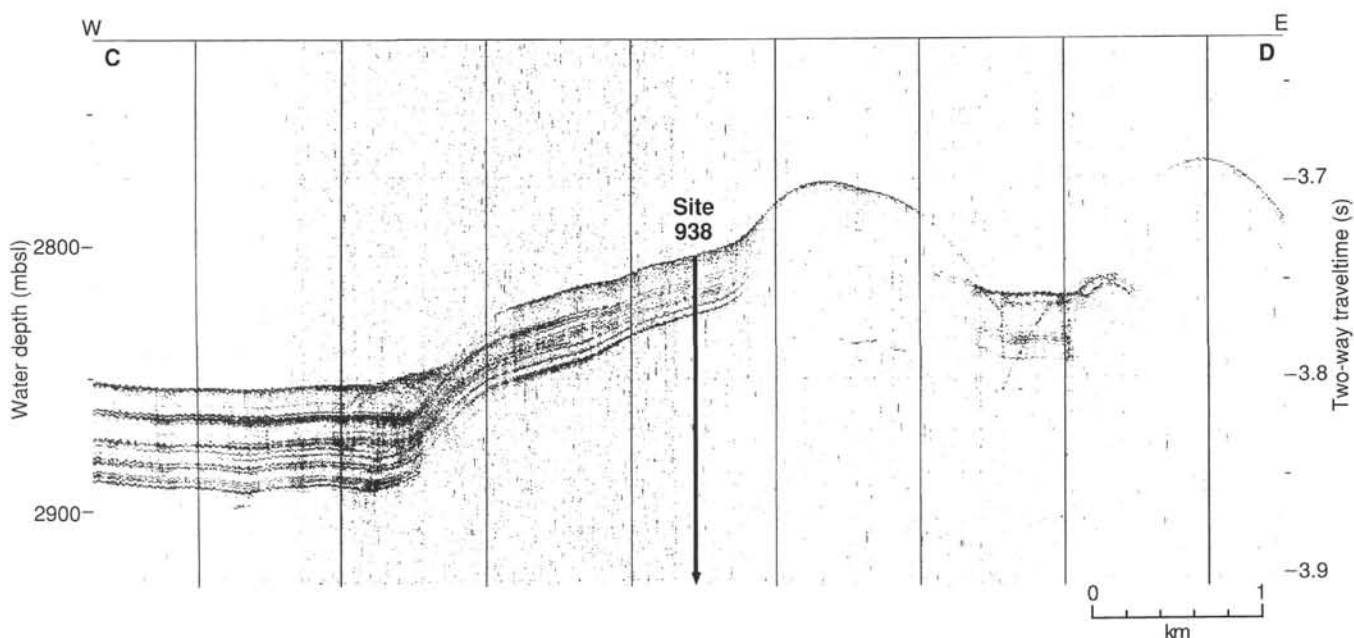


Figure 2. A 3.5-kHz profile through Site 938. Section is located as C–D on Figure 1 of the “Site 937” chapter, this volume.

4. To sample the sediment sequence that lies atop the Channel 6 levee to determine if it has a biogenic record.
5. To sample the sediment of the Channel 6 levee in an upper fan setting for comparison to the samples acquired at Site 932 on the middle fan.

OPERATIONS

Transit: Site 937 to Site 938 (AF-16)

We transited the 7 nmi from Site 937 to 938 (AF-16) in dynamic positioning (DP) mode. At 0330 hr 29 April, we deployed a beacon at 4°39.503'N, 47°18.731'W, a position determined during the seismic-reflection survey conducted prior to drilling Site 937.

Hole 938A

We used the same BHA as at Site 937, since we transited in DP mode and did not retrieve the drill string. We positioned the bit at 2813.5 mbrf and spudded Hole 938A at 0535 hr 29 April. The distance from sea level to rig floor, which depends on the ship's draft, was 11.26 m for Holes 938A and 938B. Core 1H recovered 7.60 m of sediment, and the mud line was defined to be at 2815.4 mbrf (Table 1). Cores 1H through 9H were taken from 2815.4 to 2899.0 mbrf (0–83.6 mbsf), recovering 90.73 m of sediment (108.5%). Overpull was 40,000 lb on Core 9H. Cores 3H through 9H were oriented using the Tensor tool. ADARA heat-flow measurements were made during Cores 6H and 9H.

XCB Cores 10X through 33X were taken from 2899.0 to 3125.6 mbrf (83.6–309.2 mbsf), coring 225.6 m and recovering 150.87 m (66.9%). The overall APC/XCB recovery was 77.8%. Parts of Cores 4H, 5H, 6H, 7H, 9H, 23X, and 25X were disturbed as a result of either gas-induced extrusion of core from the liner onto the rig floor or collapse of core liners.

The PCS was run in an effort to obtain a sample at in-situ pressure. Core 34P was taken at 3124.4–3125.4 mbrf (309.0–310.0 mbsf) with no recovery. The 1.0-m core was cut in 6 min with 10,000-lb wob at 80 rpm with 125–250 amps torque. We circulated a minimal 50 gpm at 125 psi for the first 0.5 m and then drilled the final 0.5 m with only

minimal circulation (to wash cuttings away to allow the bit to advance). The ball valve had not actuated; therefore, in-situ pressure was not maintained. No core was recovered. Only a trace of mud was noted above the catcher diaphragm.

Hole 938B

We moved the ship 20 m to the west, positioned the bit at 2811.0 mbrf, and spudded Hole 938B at 1920 hr 30 April. Core 1H recovered 5.28 m, and the mud line was defined to be at 2815.3 m. Cores 1H through 9H were taken from 2815.3 to 2896.6 mbrf (0–81.3 mbsf) and recovered 79.53 m (97.8%). No heat-flow measurements were made, and the cores were not oriented. The core barrel did not appear to make a full stroke while taking Cores 7H, 8H, and 9H. Parts of Cores 4H, 6H, and 8H were disturbed as a result of either gas-induced extrusion of core from the liner onto the rig floor or collapse of core liners. The bit cleared the seafloor at 0120 hr, cleared the rig floor at 0650 hr 1 May, and the beacon was recovered.

A drill-string magnetic overprint had been inferred in the XCB cores (similar results had been observed during Leg 154; Curry, Shackleton, Richter, et al., in press). The magnetic field strength of the PDC bit, float valve, both XCB shoes, spacer subs, and core catchers was measured. A small, 2–10 Oersted (Oe) reading was obtained everywhere except against the facing on the XCB shoe teeth, which measured 50 Oe. The XCB shoes were demagnetized to see if any change was noted.

LITHOSTRATIGRAPHY

Introduction

Site 938 is located on the upper fan on the flank of the levee of the abandoned Blue Channel-levee System. Hole 938A recovered sediment from a maximum depth of 306.35 mbsf with virtually complete recovery from the seafloor to 101.72 mbsf. Below 101.72 mbsf, recovery was variable downhole ranging from 6% to 96% (Fig. 3). Problems resulting from liner implosion during coring, complicated by the subsequent difficulties in extracting the core liner from the core barrel, caused extensive disruption and disorientation of sedi-

Table 1. Site 938 coring summary.

Core	Date (1994)	Time (UTC)	Depth (mbsf)	Length cored (m)	Length recovered (m)	Recovery (%)
155-938A-						
1H	April 29	0955	0.0–7.6	7.6	7.60	100.0
2H	April 29	1055	7.6–17.1	9.5	10.31	108.5
3H	April 29	1150	17.1–26.6	9.5	10.18	107.1
4H	April 29	1250	26.6–36.1	9.5	10.77	113.3
5H	April 29	1350	36.1–45.6	9.5	10.53	110.8
6H	April 29	1455	45.6–55.1	9.5	10.73	112.9
7H	April 29	1550	55.1–64.6	9.5	10.69	112.5
8H	April 29	1635	64.6–74.1	9.5	10.12	106.5
9H	April 29	1740	74.1–83.6	9.5	9.80	103.0
10X	April 29	1850	83.6–93.1	9.5	8.75	92.1
11X	April 29	1950	93.1–102.7	9.6	8.62	89.8
12X	April 29	2045	102.7–112.4	9.7	7.80	80.4
13X	April 29	2140	112.4–122.0	9.6	7.50	78.1
14X	April 29	2230	122.0–131.6	9.6	6.84	71.2
15X	April 29	2325	131.6–141.2	9.6	7.44	77.5
16X	April 30	0020	141.2–150.8	9.6	7.80	81.2
17X	April 30	0115	150.8–160.4	9.6	5.08	52.9
18X	April 30	0215	160.4–170.1	9.7	5.95	61.3
19X	April 30	0305	170.1–179.8	9.7	2.70	27.8
20X	April 30	0415	179.8–189.5	9.7	7.56	77.9
21X	April 30	0525	189.5–196.5	7.0	0.46	6.6
22X	April 30	0625	196.5–203.5	7.0	6.92	98.8
23X	April 30	0735	203.5–213.1	9.6	5.23	54.5
24X	April 30	0835	213.1–222.8	9.7	7.65	78.8
25X	April 30	0940	222.8–232.3	9.5	2.81	29.6
26X	April 30	1045	232.3–241.8	9.5	2.05	21.6
27X	April 30	1155	241.8–251.4	9.6	9.27	96.5
28X	April 30	1305	251.4–261.0	9.6	7.90	82.3
29X	April 30	1420	261.0–270.6	9.6	8.28	86.2
30X	April 30	1540	270.6–280.2	9.6	5.77	60.1
31X	April 30	1705	280.2–289.9	9.7	4.81	49.6
32X	April 30	1830	289.9–299.5	9.6	7.91	82.4
33X	April 30	1940	299.5–309.2	9.7	6.85	70.6
34P	April 30	2040	309.2–310.2	1.0	0.00	0.0
Coring totals				310.2	242.7	78.20
155-938B-						
1H	April 30	2320	0.0–5.3	5.3	5.28	99.6
2H	April 30	2355	5.3–14.8	9.5	10.00	105.2
3H	May 1	0035	14.8–24.3	9.5	10.31	108.5
4H	May 1	0110	24.3–33.8	9.5	10.20	107.8
5H	May 1	0150	33.8–43.3	9.5	10.16	106.9
6H	May 1	0230	43.3–52.8	9.5	9.84	103.0
7H	May 1	0305	52.8–62.3	9.5	6.47	68.1
8H	May 1	0345	62.3–71.8	9.5	7.08	74.5
9H	May 1	0435	71.8–81.3	9.5	10.19	107.2
Coring totals				81.3	79.5	97.90

Note: An expanded version of this coring summary table that includes lengths and depths of sections, location of whole-round samples, and comments on sampling disturbance is included on the CD-ROM in the back pocket of this volume.

ment in the intervals from 36.10 to 38.90 mbsf (Sections 938A-5H-1 through -2) and from 55.10 to 74.72 mbsf (Sections 938A-7H-1 through -8H-CC). Hole 938B extended to 81.99 mbsf and recovered most of these two disturbed intervals; minor problems resulted in a lack of recovery or sediment disruption only in the interval from 59.27 to 69.03 mbsf (interval 938B-7H-CC, 34 cm, through -8H-CC, 31 cm). In addition, expansion of methane gas during core recovery commonly affected the sediment by disrupting the primary sedimentary structures in many silt and sand beds, and by producing void spaces within many of the core sections (see "Lithostratigraphy" section in the "Explanatory Notes" chapter, this volume).

Description of Lithostratigraphic Units

Unit I

Interval: 155-938A-1H-1, 0–44 cm; 155-938B-1H-1, 0–42 cm
Age: Holocene
Depth: 0.00–0.44 mbsf

Unit I consists of a brown (10YR 5/3) foraminifer-nannofossil clay from 0.00 to 0.38 mbsf overlying a light olive brown (2.5Y 5/4) diagenetic iron-rich crust that marks the base of Unit I at this site. Similar diagenetic, iron-rich layers or crusts have been analyzed pre-

viously and correlated throughout the Amazon Fan and adjacent Guiana Basin (e.g., Damuth, 1977; see "Introduction" chapter, this volume). The calcareous clay above the iron-rich crust commonly shows burrow mottling and has a carbonate content of 33% at 0.08 mbsf (see "Organic Geochemistry" section, this chapter).

Unit II

Intervals: 155-938A-1H-1, 44 cm, through -33X-CC, 22 cm; 155-938B-1H-1, 42 cm, through -9H-CC, 32 cm
Age: Holocene to late Pleistocene
Depth: 0.44–306.35 mbsf

Unit II consists predominantly of terrigenous silty clay ranging in color from dark gray (5Y 4/1) through dark olive gray (5Y 3/2) to very dark gray (5Y 3/1). Intervals with common to abundant laminae and thin beds of silt and very fine sand alternate with intervals having less than one silt layer per meter (Figs. 3 and 4). The carbonate content of Unit II shows downhole variability generally in the range of 1% to 5% except for higher values around 120 to 150 mbsf.

Distinct color banding, burrows, mottles (on a centimeter scale), and friable micronodules (approximately 1-mm scale) occur in varying abundance throughout much of Unit II and are generally black (N2/0) where color boundaries are sharp, but 5Y 2.5/1 where less distinct in both contrast and boundaries). These black stains are caused by diagenetic hydrotroilite, which imparts an ephemeral black color (N2/0) to the sediment (see "Introduction" chapter, this volume). In general, darker banding and mottles do not appear to be associated with particular detrital grain sizes, although in some cases laminae and beds of silt are heavily stained (see silt bed at 145 cm in the whole-core photograph that includes Section 938A-2H-2 in the "Cores" chapter, this volume). The contrast between the hydrotroilite-stained features and the host silty clay generally decreases downhole because the dominant sediment color becomes darker (i.e., very dark gray, 5Y 3/1). Unit II is subdivided into subunits based on the frequency of occurrence of common silt laminae, thin silt beds, and sandy silt or silty sand beds (Figs. 3 and 4).

Subunit IIA

Subunit IIA extends from the base of Unit I at 0.44 mbsf to 10.55 mbsf (interval 938A-1H-1, 44 cm, through 938A-2H-2, 145 cm). This subunit consists of dark gray (5Y 4/1) clay with distinct black (N2/0) mottles and burrows (e.g., Section 938A-1H-2). The sediment changes downhole to a dark olive gray (5Y 4/1 to 5Y 3/2) silty clay with less distinct mottles. The two carbonate determinations in this subunit are 1.5% and 5.1%.

Subunit IIB

Subunit IIB extends from 10.55 to 71.84 mbsf (interval 938A-2H-2, 145 cm, through 938A-8H-5, 139 cm) and is characterized by dark olive gray (5Y 3/2) to dark gray (5Y 3/1) silty clay with irregularly spaced silt laminae and a few beds that grade from very fine sand at the base (Figs. 4 and 5). Overall, this subunit averages about one lamina or bed per meter with only two short intervals of higher frequency (to six layers per meter in interval 938A-3H-2, 24–123 cm, and to four per meter in interval 938A-6H-4, 136 cm, through -7, 119 cm). There is no recognizable trend in the frequency of silt laminae through this subunit, and there are intervals as much as 5 m thick with no silt beds. Burrow mottling is present throughout most of the subunit except where color banding is prominent between 55.40 and 65.11 mbsf (interval 938A-7H-1, 30 cm, through -8H-1, 51 cm). The carbonate content averages about 2% with only one determination exceeding 2.5%.

Subunit IIC

Subunit IIC extends from the base of Subunit IIB (71.84 mbsf) to 117.45 mbsf (interval 938A-8H-5, 139 cm, through -13X-4, 55 cm). This subunit consists of dark to very dark gray (5Y 4/1 to 5Y 3/1)

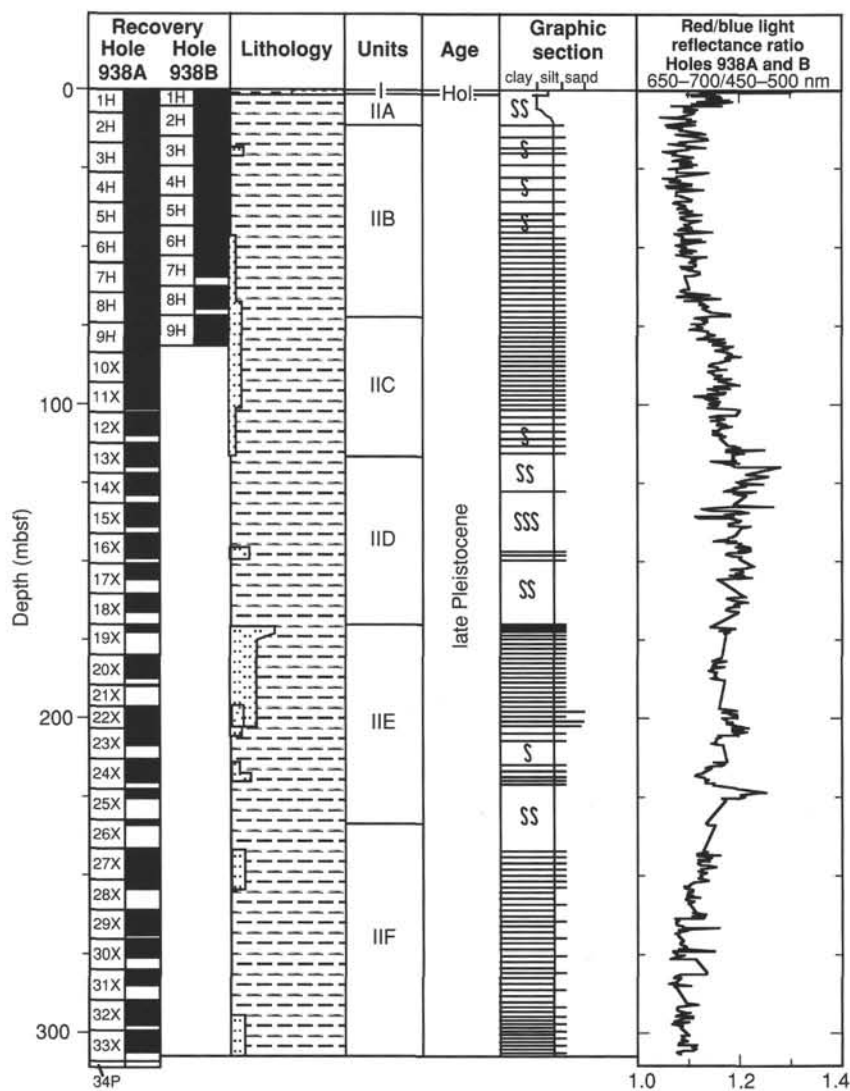


Figure 3. Composite stratigraphic section for Site 938 showing core recovery in both holes, a simplified summary of lithology, depths of unit boundaries, age, a graphic section with generalized grain-size and bedding characteristics, and downhole variations in light-reflectance values. The lithologic symbols are explained in Figure 1 of the "Explanatory Notes" chapter, this volume. The light-reflectance profile is a composite record based on Hole 938B, 0 to 77 mbsf, and Hole 938A, 77 to 306 mbsf (intervals 155-938B-1H-1, 0 cm, through -9H-4, 70 cm, and 155-938A-9H-3, 17 cm, through -33X-CC).

silty clay with numerous silt laminae and beds of silt and very fine sand (Fig. 6). Sand beds are as thick as 9 cm. Parallel lamination was observed in many beds as well as in a few laminae thicker than 5 mm. Cross-lamination in sand and silt beds is common only within a few short intervals (e.g., interval 938A-10X-6, 144 cm, through -10X-7, 55 cm; Fig. 6). Burrow mottles are common in this subunit, and many silt laminae are disrupted or discontinuous as a result of crosscutting burrows (Fig. 7). The carbonate content of Subunit IIC is approximately 3%; the lowest value measured is greater than the Subunit IIB average.

Subunit IID

Subunit IID extends from 117.45 to 170.53 mbsf (interval 938A-13X-4, 55 cm, through -19X-1, 43 cm) and consists of dark olive gray (5Y 3/2) to very dark gray (5Y 3/1) silty clay that contains approximately one silt or sandy-silt laminae every two meters. Most of this subunit shows mottles and burrows; rare siderite concretions are also present. The silt laminae are not uniformly distributed through the subunit (Fig. 4). Two-thirds of the silt laminae occur within one short interval between 145.44 and 148.83 mbsf (interval 938A-16X-3, 124 cm, through -16X-CC). At the other extreme (and immediately above the "silty" section), intervals with no silt layers are as thick as 9 m (interval 938A-15X-4, 10 cm, through -16X-3, 124 cm). The carbonate

content averages nearly 6%, which is more than double other subunits. The highest value of 18.9% is from a layer of uncertain origin (Sample 938A-14X-4, 67–68 cm).

Subunit IIE

The top of Subunit IIE, which extends from 170.53 to 233.73 mbsf (interval 938A-19X-1, 43 cm, through -26X-1, 143 cm), is placed where there is an abrupt increase in the number of laminae and beds of silt. More than 120 laminae and beds of silt compose about 25% of the uppermost 2.62 m of this subunit. The frequency of discrete silt layers decreases in the lower part of the subunit, but there is more sand present. Recovery of this subunit was the lowest in Hole 938A (just under 50%), suggesting that more of the unrecovered section might contain sand beds. The carbonate content of this subunit is less than 2.4%, which is substantially lower than the overlying Subunit IID.

Subunit IIF

Subunit IIF extends from the base of Subunit IIE (233.73 mbsf) to the bottom of Hole 938A at 306.35 mbsf (interval 938A-26X-1, 143 cm, through -33X-CC, 22 cm) and consists of very dark gray (5Y 3/1) silty clay with irregularly spaced laminae and beds of silt. Many of the silt layers have been disrupted during coring; silt laminae are

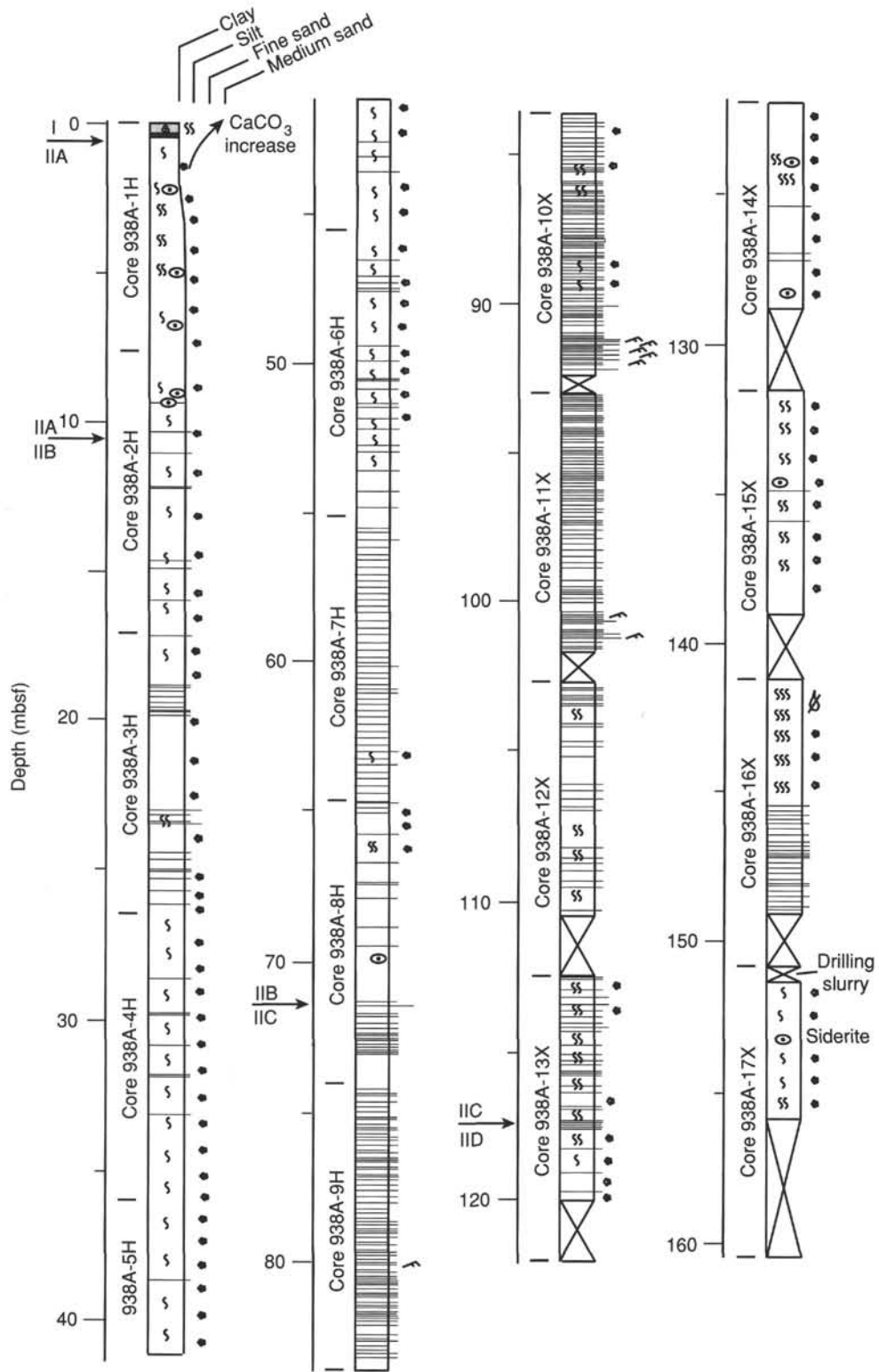


Figure 4. Graphic sedimentological columns for Site 938 showing grain-size variation (width of columns), bed thickness, and sedimentary structures; symbols and preparation of these columns are explained in the "Lithostratigraphy" section of the "Explanatory Notes" chapter, this volume. Arrows indicate the positions of unit and subunit boundaries. The upper part of the column is shown in the strike section of the foldout (back pocket, this volume) for comparison of levee sequences on the middle and upper fan.

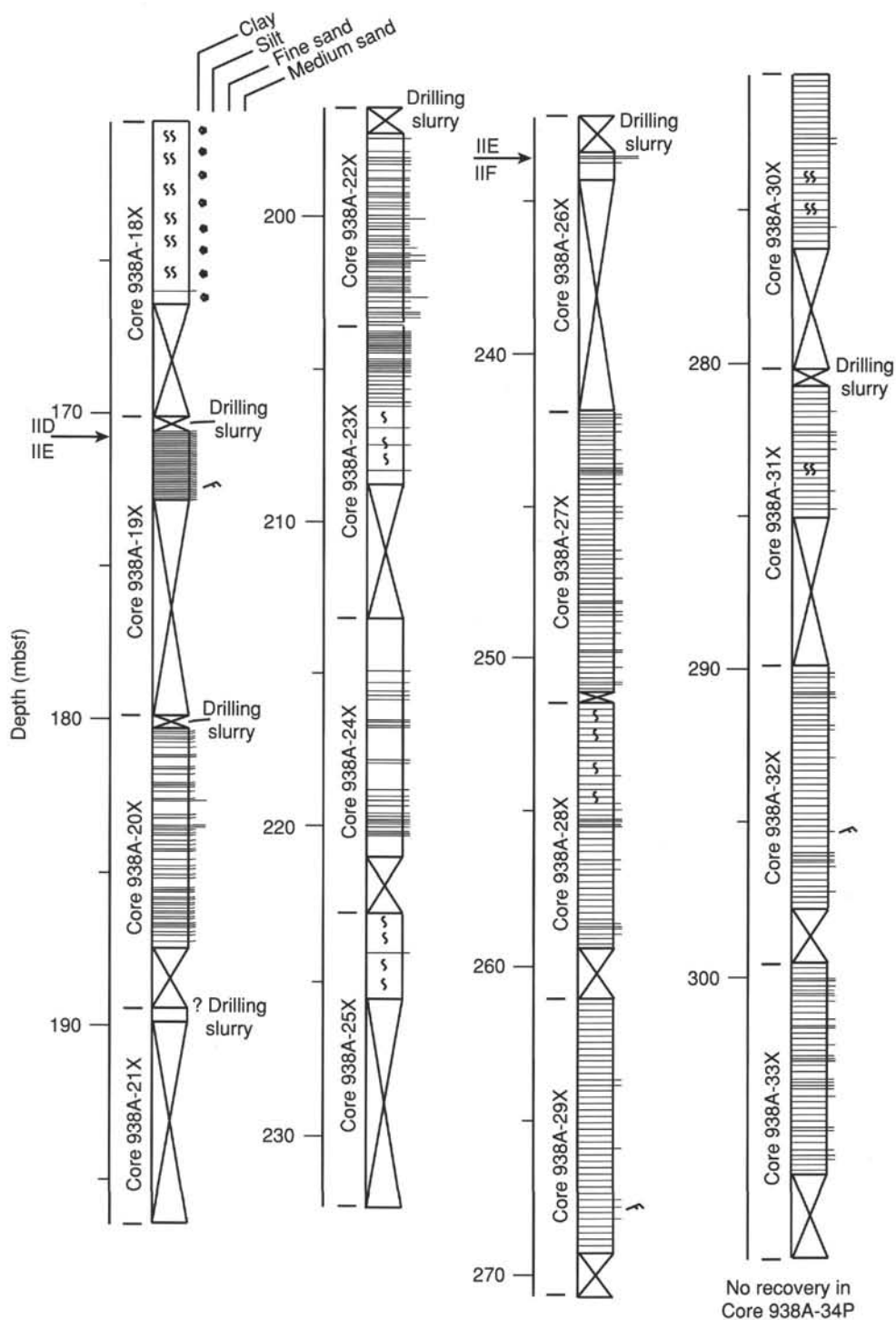


Figure 4 (continued).

commonly discontinuous across the width of the core. The thicker laminae and beds of silt in this subunit that still exhibit primary sedimentary structures show typical Bouma turbidite divisions (T_{cde} and T_{de} ; Fig. 8). The number of beds per meter decreases from three in Core 938A-27X at the top of the unit to 0.5 in Cores 938A-29X and -30X. Below Core 938A-30X, the ratio then increases downhole to three beds per meter in Core 938A-33X. The distribution of silt layers in this subunit differs from that in Subunits IIB and IID in two respects: there are no long intervals without silt laminae, and only a few intervals that are tens of centimeters in length have numerous silt lay-

ers. Subunit IIF is the most consistently color-banded sequence in Hole 938A (Fig. 4). The average carbonate content is more than 3%, exceeded only by Subunit IID and Unit I.

Mineralogy

Mineralogy was determined by estimation of mineral volume percentages in smear slides and by X-ray diffraction (XRD) analysis of samples from silt layers.

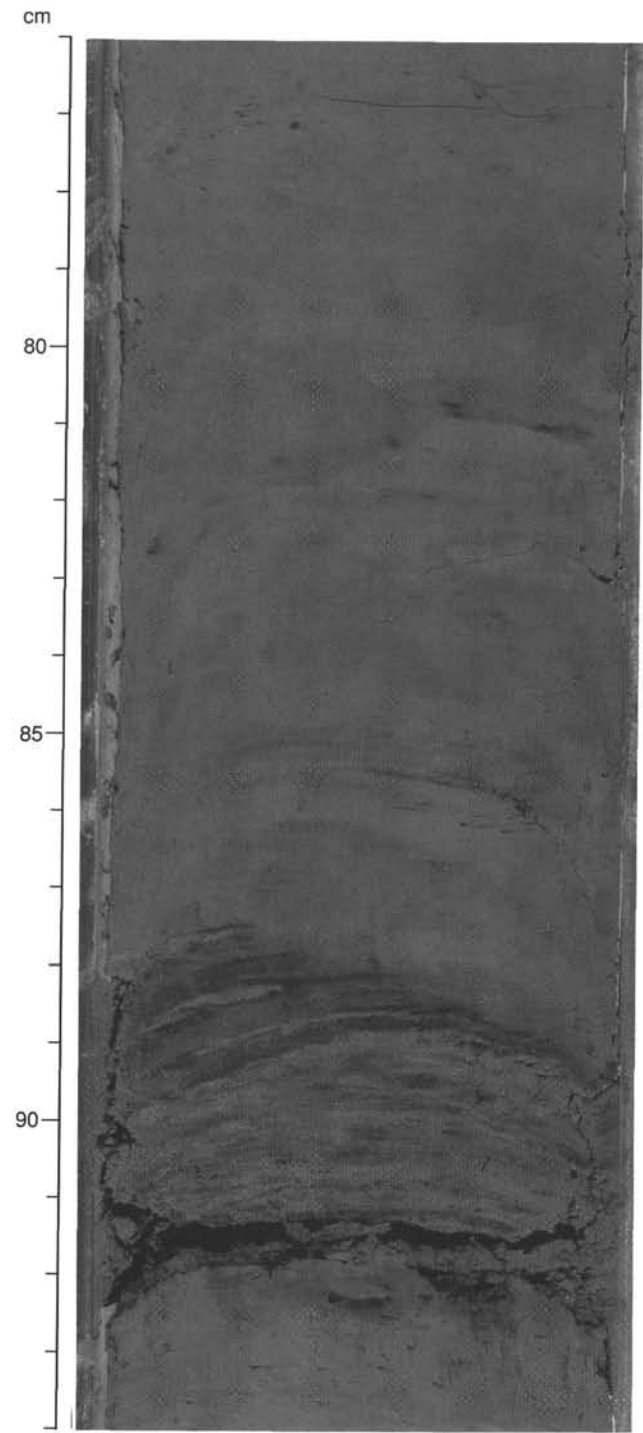


Figure 5. Truncated laminae in a graded bed of very fine sand to silt (87 to 92 cm). The surrounding sediment is burrowed silty clay of Subunit II B (interval 155-938A-3H-5, 76–94 cm).

Smear-slide Synthesis

Silty clay is the dominant lithology of Unit II; the silt fraction consists of about 70% quartz (mainly monocrystalline), 10% feldspar (mainly plagioclase), 5% mica, and 10% accessory minerals. The accessories include common hornblende, augite, hypersthene and opaques, and rare zircon, spinel, and monazite. Organic detritus, foraminifers, and sponge spicules compose less than 5%, and nannofos-

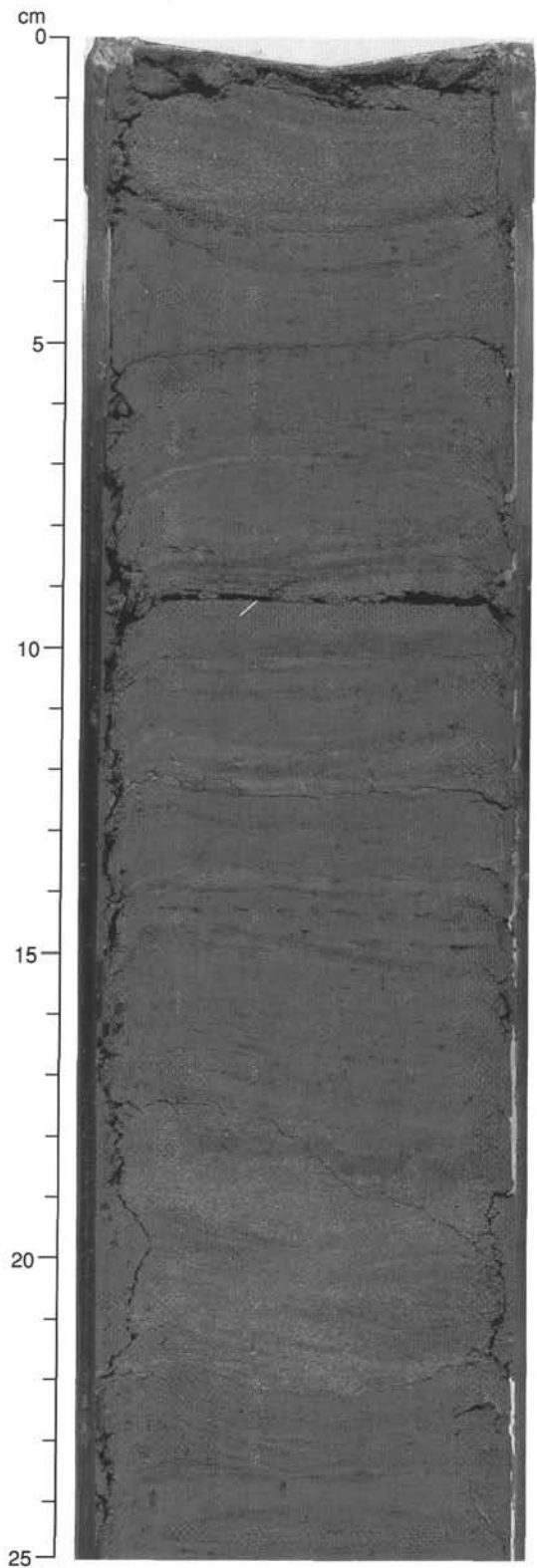


Figure 6. Laminae and beds of very fine sand showing cross-lamination (Bouma T_{cd}) from Unit IIC (interval 155-938A-10X-7, 0–25 cm).

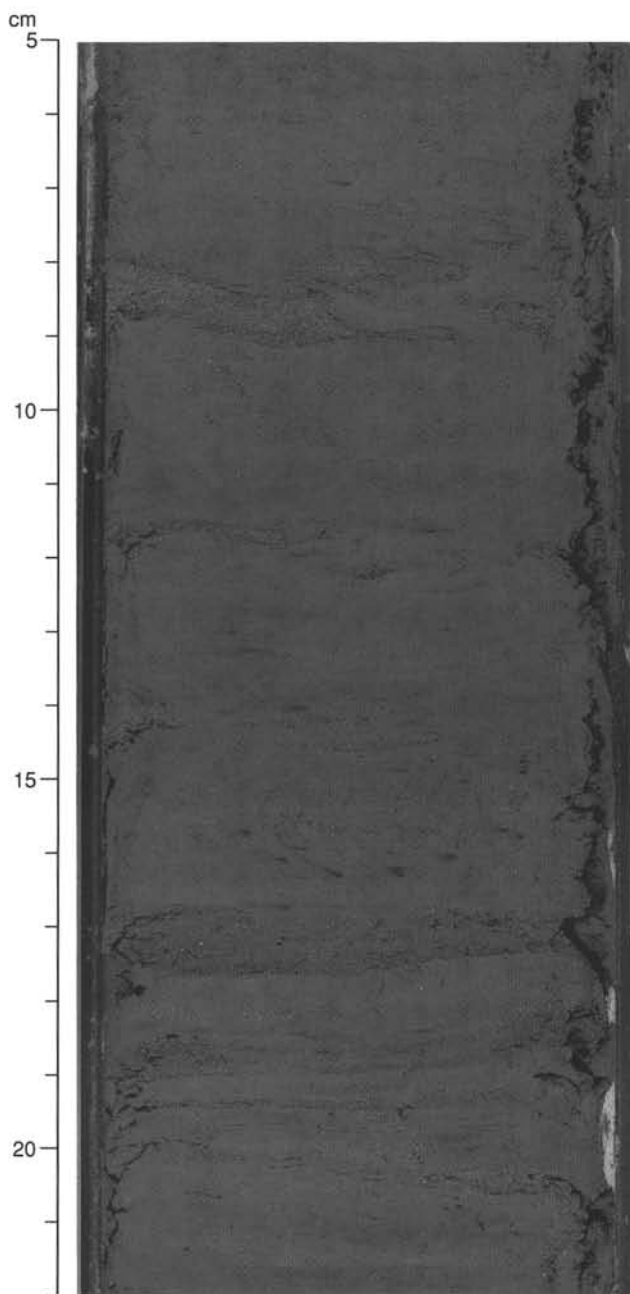


Figure 7. Examples of large horizontal burrows with *Spreiten* (15 to 16 cm) and silt laminae (8 to 9 cm) disrupted by burrowing in Subunit II C (interval 938A-13X-3, 5–22 cm).

sils compose less than 5% in nearly all samples. The components of the silty fraction show no significant changes between the six subunits of Unit II.

XRD Data

Bulk XRD analysis was performed on samples of silty clay from Cores 938A-1H through -33X (Table 2). The common minerals throughout the cored succession, based on the relative intensities of their primary peaks (normalized to quartz intensity), are quartz, plagioclase, K-feldspar, augite, and the clay minerals smectite, illite (+ mica), and kaolinite (Fig. 9A). A few samples contain calcite and cal-

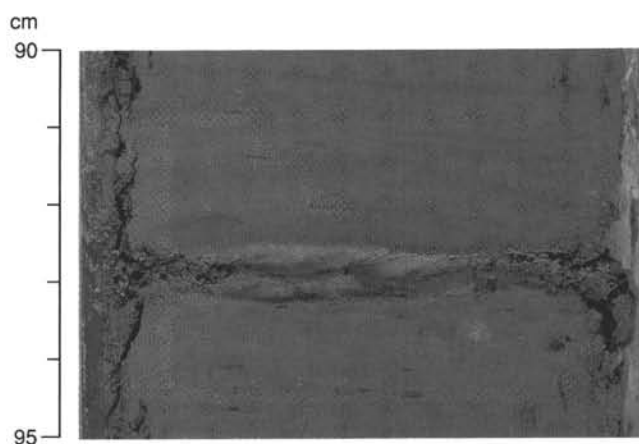


Figure 8. Turbidite silt bed in Subunit IIF showing Bouma T_{cde} sequence (interval 938A-32X-4, 90–95 cm).

ic amphibole, which is probably hornblende based on its presence in smear-slide samples. Illite (+ mica) has the highest relative peak intensity and largest variation among the clay minerals. Total clay minerals (+ mica) increase from 20 to 40 mbsf and then generally decrease in relative abundance from 40 to 200 mbsf (Fig. 9A); farther downhole there is a general increase from 260 to 300 mbsf. These trends basically reflect the illite (+ mica) intensities of the total clay component (Fig. 9B). Total feldspar and hornblende + augite intensities do not vary much with depth.

Spectrophotometry

Light-reflectance levels of the brown calcareous clay in Unit I reach 35%, whereas those of the dark olive gray to very dark gray sediment in Unit II range between 15% and 25%. The ratio between red (650–700 nm) and blue (450–500 nm) spectral reflectance averages 1.14 (Fig. 3). The highest red/blue ratio is measured in the brownish gray calcareous clay of Unit I, reflecting the enhancement of red reflectance caused by iron oxyhydroxides. The lowest red/blue ratios are obtained from the intensively black mottled and color-banded silty clay in Subunits IIB and IIF (e.g., below 260 mbsf); the higher ratios roughly correspond to the sediment intervals characterized by a greater abundance of silt layers and less extensive black mottling and color banding (e.g., Subunits IIC and IIE). Similar to the spectrophotometry results at Site 937, the variability in the red/blue ratio observed throughout Unit II presumably reflects changes in the amount of diagenetic hydrotroilite.

Discussion

Two major lithologic patterns are observed in the sediment at this site: (1) differences in the relative abundance of silt and sand layers, and (2) apparent trends in the vertical succession of “silt-rich” and “silt-poor” sequences. Subunits of Unit II are distinguished on the relative abundance of sand and silt layers. These subunits indicate several cycles of deposition at Site 938 (Fig. 4). Subunits IIB, IID, and IIF are 50- to 70-m-thick intervals that have relatively few silt or sand beds (or laminae) and exhibit a general hemipelagic character. Subunit IID corresponds to the upper part of the interval of deposition related to the Channel 6 and Yellow Channel-levee System (see “Core-Seismic Integration” section, this chapter). Color banding is common to Subunits IID and IIF, whereas burrows and mottling are common in IIB and IID. Excluding the uppermost 10 m of sediment at Site 938, Subunits IID and IIF have the highest carbonate content. The relative paucity of coarse-grained components in these intervals

Table 2. Relative peak intensities of the main minerals in representative samples for most cores recovered at Site 938.

Core, section, interval (cm)	Depth (mbsf)	Relative intensity of primary peaks								
		Smectite	Mica + Illite	Kaolinite	Quartz	Plagioclase	K-feldspar	Augite	Hornblende	Calcite
155-938A-										
1H-5, 130-131	7.30	6.2	16.1	7.9	100.0	8.7	*	3.0	*	*
2H-6, 7-8	15.17	3.7	7.7	4.0	100.0	8.5	4.5	1.7	0.5	*
3H-5, 43-44	23.53	2.5	7.3	3.9	100.0	16.5	5.3	1.2	*	*
4H-6, 11-13	33.12	8.4	21.0	13.4	100.0	10.1	10.5	3.2	*	*
5H-2, 50-51	38.10	8.2	28.6	13.2	100.0	9.3	*	3.4	*	*
6H-6, 4-5	51.88	6.9	20.8	10.7	100.0	8.4	*	3.1	*	*
7H-6, 40-41	61.28	8.6	16.7	10.0	100.0	9.1	3.9	2.1	*	*
8H-1, 3-4	64.63	5.3	6.6	3.9	100.0	9.0	3.2	1.3	0.7	*
9H-6, 8-9	80.21	9.6	16.7	10.1	100.0	11.9	4.5	1.9	0.8	*
10X-3, 93-94	86.70	6.0	16.9	8.1	100.0	9.5	7.4	2.1	*	*
11X-1, 16-17	93.26	3.9	6.8	4.5	100.0	11.4	3.2	1.1	1.3	*
12X-5, 50-51	109.20	12.5	13.8	10.7	100.0	9.1	5.1	2.4	*	*
13X-3, 42-44	115.82	6.1	12.8	8.3	100.0	12.1	4.0	1.6	*	1.9
14X-3, 36-37	125.36	4.0	9.6	5.0	100.0	6.6	4.5	1.6	*	*
15X-3, 138-139	135.84	2.2	11.9	5.0	100.0	9.3	6.4	4.2	*	1.3
16X-5, 86-87	148.06	5.8	11.8	7.9	100.0	8.9	4.7	2.0	*	*
17X-1, 47-48	151.27	5.6	8.3	4.9	100.0	7.2	3.4	2.0	1.1	*
18X-3, 57-58	163.45	8.7	15.5	5.5	100.0	8.9	*	2.0	*	*
19X-2, 68-69	172.28	3.3	8.5	4.6	100.0	7.1	3.8	1.2	*	*
20X-3, 133-134	184.13	3.1	8.5	4.0	100.0	10.0	5.2	1.4	1.8	*
22X-2, 80-81	198.80	3.1	7.5	4.0	100.0	11.0	4.9	0.9	*	*
23X-1, 140-141	204.90	2.5	7.7	3.5	100.0	11.3	3.7	1.3	0.9	*
24X-5, 52-53	219.62	3.1	11.8	7.0	100.0	9.1	4.0	1.4	*	*
25X-2, 130-131	224.67	5.0	14.6	7.5	100.0	9.6	4.0	1.9	*	*
26X-1, 134-135	233.64	3.7	6.9	3.1	100.0	16.7	5.1	0.7	1.5	*
27X-3, 51-52	245.31	3.0	8.3	4.9	100.0	7.3	3.6	1.6	*	*
28X-2, 84-85	253.74	4.4	8.6	4.6	100.0	8.5	7.1	1.4	*	*
29X-4, 43-44	265.93	2.1	5.6	3.2	100.0	7.7	2.8	1.4	0.5	*
30X-3, 56-57	274.16	6.3	14.9	7.5	100.0	10.6	7.0	2.0	*	*
31X-2, 56-57	282.26	4.1	11.1	5.9	100.0	11.5	4.2	1.5	*	*
32X-5, 53-54	296.43	6.3	19.2	10.4	100.0	9.3	4.8	1.9	*	*
33X-5, 4-5	305.54	7.8	15.7	6.9	100.0	13.4	3.6	1.4	*	*

Notes: See "Lithostratigraphy" section in the "Explanatory Notes" chapter, this volume, for XRD methods. * = non-detection.

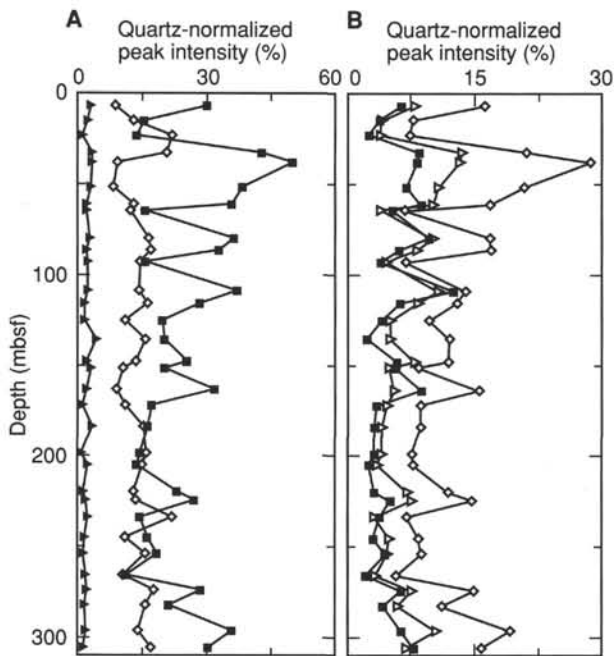


Figure 9. Relative abundance of silicate minerals in silty clay samples, based on XRD analysis (Table 2). **A.** Plot against depth of the relative peak intensities of the main mineral groups. Squares = clay minerals + mica; diamonds = feldspar; triangles = augite + hornblende. **B.** Plot against depths of the ratios of the peak intensities of clay minerals and micas. See text for discussion. Squares = smectite; diamonds = (illite + mica); triangles = kaolinite.

compared to Subunits IIC and IIE indicates major lateral shifts in the loci of coarse-sediment deposition and/or a reduced frequency or size of turbidity currents during the periods when these subunits were deposited.

Both the "silt-rich" and "silt-poor" subunits show some internal variation suggesting changing depositional patterns on an even finer scale. Subunit IIB appears to have at least three cycles of alternation between intervals with very rare silt units and intervals with 10 to 20 silt laminae or beds per meter. These intervals are 5 to 15 m thick. Subunit IID is 60 m of dominantly bioturbated silty clay but has one interval of numerous silt beds as described above. Subunit IIF shows downhole changes in the number of silt layers per meter from three to less than one and back to three at the bottom.

There may be three sequences of turbidite deposition in Subunit IIE suggesting three separate pulses of levee growth; this subunit corresponds to the upper part of the Channel-levee System 6. These pulses are separated by silty clay sections. The upper sequence extends from the top of the subunit at 170.53 mbsf to the top of a silty clay section with few silt laminae at 205.08 mbsf (interval 938A-23X-2, 8 cm). The middle sequence includes the silty clay interval whose top is at 205.08 mbsf and extends to the upper boundary of another silty clay with only one silt layer at 222.80 mbsf (interval 938A-25X-1, 0 cm). The lowest sequence includes this silty clay and extends to the bottom of Subunit IIE, which is the base of the deepest recovered sand bed at 233.73 mbsf (interval 938A-26X-1 at 143 cm).

The lowermost part of Subunit IIC is a 7-m-thick interval with about six laminae and beds of silt or sand per meter. Above this basal interval is a 20-m-thick coarsening-upward sequence that extends to a sand bed at 90.14 mbsf (interval 938A-10X-6, 14 cm). The uppermost 20 m of this subunit (above 90 mbsf), in contrast, shows fairly uniform abundance in the number of silt layers (averaged over intervals greater than 1 m) until the abrupt reduction in turbidite deposition of silt that marks the top of this subunit. Subunit IIC thus appears to represent a levee progradation phase with an initial high frequency

Table 3. Calcareous nannofossil and siliceous microfossil abundance data for Hole 938A.

Core, section, interval (cm)	Top interval (mbsf)	Bottom interval (mbsf)	Calcareous nannofossils			Diatoms				Ericson Zone (inferred from foraminifers)	Age (inferred from foraminifers)
			Abundance	Preservation	Zone	Marine	Freshwater	Sponge spicules	Radiolarians		
155-938A-											
1H-MI, 0	0.00		a	g	CN15b	vr	b	f	b	Z	Holocene
1H-CC, 18-19	7.59	7.60	b	—		b	b	b	b	Z	Holocene?
2H-CC, 29-30	17.90	17.91	b	—		b	b	b	b	Y	late Pleist.
3H-CC, 29-30	27.27	27.28	b	—		b	b	b	b	Y	late Pleist.
4H-CC, 47-48	37.36	37.37	tr	—		b	b	r	b	Y	late Pleist.
5H-CC, 54-55	45.27	45.28	tr	—		b	b	b	b	Y	late Pleist.
6H-CC, 61-62	56.32	56.33	vr	—		b	b	b	b	Y	late Pleist.
7H-5, 84	60.84		b	—		b	b	b	b	Y	late Pleist.
7H-CC, 69-70	61.57	61.58	vr	—		b	b	b	b	Y	late Pleist.
8H-2, 19	66.29		r	—		b	b	a	b	Y	late Pleist.
8H-3, 22	67.82		vr	—		b	b	a	b	Y	late Pleist.
8H-5, 15	70.60		b	—		b	b	b	b	Y	late Pleist.
8H-5, 63	71.08		tr	—		b	b	c	b	Y	late Pleist.
8H-CC, 102-103	74.71	74.72	b	—		b	b	b	b	Y	late Pleist.
9H-CC, 33-34	83.27	83.28	b	—		b	b	b	b	Y	late Pleist.
10X-CC, 21-22	92.34	92.35	b	—		b	b	b	b	Y	late Pleist.
11X-CC, 19-20	101.71	101.72	tr	—		b	b	b	b	Y	late Pleist.
12X-CC, 22-23	110.49	110.50	b	—		b	b	b	b	Y	late Pleist.
13X-CC, 32-33	119.89	119.90	b	—		b	b	vr	b	Y	late Pleist.
14X-CC, 21-22	128.83	128.84	tr	—		b	b	b	b	Y	late Pleist.
15X-CC, 49-50	139.03	139.04	tr	—		b	b	b	b	Y	late Pleist.
16X-CC, 19-20	148.99	149.00	vr	—		b	b	b	b	Y _{p. obliq.}	late Pleist.
17X-2, 84-85	153.14	153.15	b	—		b	b	b	b	Y	late Pleist.
17X-CC, 22-23	155.87	155.88	vr	—		b	b	b	b	Y	late Pleist.
18X-4, 14	164.52		b	—		b	b	b	b	Y	late Pleist.
18X-CC, 81-82	166.34	166.35	b	—		b	b	b	b	Y	late Pleist.
19X-CC, 20-21	172.79	172.80	vr	—		b	b	vr	b	Y	late Pleist.
20X-CC, 22-23	187.35	187.36	b	—		b	b	r	b	Y	late Pleist.
21X-CC, 45-46	189.95	189.96	b	—		b	b	b	b	Y	late Pleist.
22X-CC, 16-17	203.41	203.42	b	—		b	b	r	b	Y	late Pleist.
23X-CC, 72-73	208.46	208.47	tr	—		b	b	b	b	Y	late Pleist.
24X-CC, 21-22	220.74	220.75	b	—		b	b	b	b	Y	late Pleist.
25X-CC, 73-74	225.60	225.61	tr	—		b	b	b	b	Y	late Pleist.
26X-CC, 11-12	234.34	234.35	b	—		b	b	b	b	Y	late Pleist.
27X-CC, 26-27	251.06	251.07	vr	—		b	b	b	b	Y	late Pleist.
28X-CC, 39-40	258.29	258.30	tr	—		b	b	b	b	Y	late Pleist.
29X-CC, 26-27	258.29	258.30	tr	—		b	b	b	b	Y	late Pleist.
30X-CC, 30-31	275.40	275.41	tr	—		b	b	b	b	Y	late Pleist.
31X-CC, 34-35	285.96	285.97	b	—		b	b	b	b	Y	late Pleist.
32X-CC, 40-41	297.80	297.81	b	—		b	b	b	b	Y	late Pleist.
33X-CC, 21-22	306.34	306.35	b	—		b	b	b	b	Y	late Pleist.

of turbidity-current events that deposited some sand-size material followed by fairly uniform conditions of deposition of silt without sand that is inferred to represent "mature" levee aggradation until the sediment supply was cut off. This subunit corresponds to the lower part of the Blue System.

BIOSTRATIGRAPHY

Calcareous Nannofossils

Calcareous nannofossils recovered at Site 938 are all from nannofossil Zone CN15b (Table 3). Nannofossils are abundant and well preserved in the nannofossil and foraminifer clay of Unit I from the mud line to 0.15 mbsf (Samples 938A-1H-1, mud line, to -1H-1, 15 cm). Nannofossil diversity is high, and the assemblage includes species of dissolution-prone genera such as *Scyphosphaera* and *Pontosphaera*. The Holocene microfossil assemblage also includes spicules of calcareous sponges. Nannofossils are rare or absent from 0.18 mbsf to the base of the hole at 306 mbsf (Samples 938A-1H-CC, 18-19 cm, through -33X-CC, 21-22 cm). All assemblages have a low diversity and are strongly affected by dissolution. Only dissolution-resistant species like *G. oceanica* and *C. leptoporus* are found in Unit II. The occurrence of *E. huxleyi* places the glacial sediment of Unit II in Zone CN15b.

Planktonic Foraminifers

Based on core-catcher samples, the boundary between Ericson Zones Z and Y (disappearance of *G. tumida*) is between Samples

938A-1H-CC, 9-18 cm (7.5 mbsf), and -2H-CC, 20-29 cm (17.8 mbsf; Table 4; Fig. 10). The Z/Y boundary may be at the bottom of Unit I, however, given the possible downhole contamination of the core-catcher samples. Planktonic foraminifers have relatively higher abundances in Unit I and Subunit IIA. Planktonic foraminifer abundances decrease to rare in Subunit IIB from 27.2 mbsf (938A-3H-CC, 20-29 cm) to the upper part of Subunit IIC at 83.3 mbsf (938A-9H-CC, 24-33 cm). Subunits IIB and IIC contain black authigenic mineral nodules, abundant calcareous spines (many of which have been identified as Echinoid spines), mica, and iron-stained foraminifers. Planktonic foraminifer abundances increase in Subunits IIC and IID (Samples 938A-10X-CC, 12-21 cm [92.3 mbsf], through -15X-CC, 40-49 cm [139 mbsf]), which also contain calcareous sponge spicules, mica, and iron-stained foraminifers. The *Y_{p. obliq.}* datum occurs at 149 mbsf (938A-16X-CC, 24-33 cm) in the middle of Subunit IID (Fig. 10), suggesting that sediment below this level is older than 40 ka. Planktonic foraminifer abundances are low between 149 mbsf (Sample 938A-16X-CC, 24-33 cm) and the base of Hole 938A at 306.3 mbsf (Sample 938A-33X-CC, 12-21 cm). Subunits IID and IIE contain sand, wood particles, mica, red authigenic nodules, and some iron-stained foraminifers. The absence of *G. menardii* and *G. tumida* below the *Y_{p. obliq.}* datum suggests that the base of Hole 938A is younger than 85 ka.

Benthic Foraminifers

Benthic foraminifers are rare or absent in Hole 938A. Abyssal benthic foraminifers occur in low abundances in the finer grained intervals of Subunits IIB and IIC from 37.4 mbsf to 92.3 mbsf (938A-

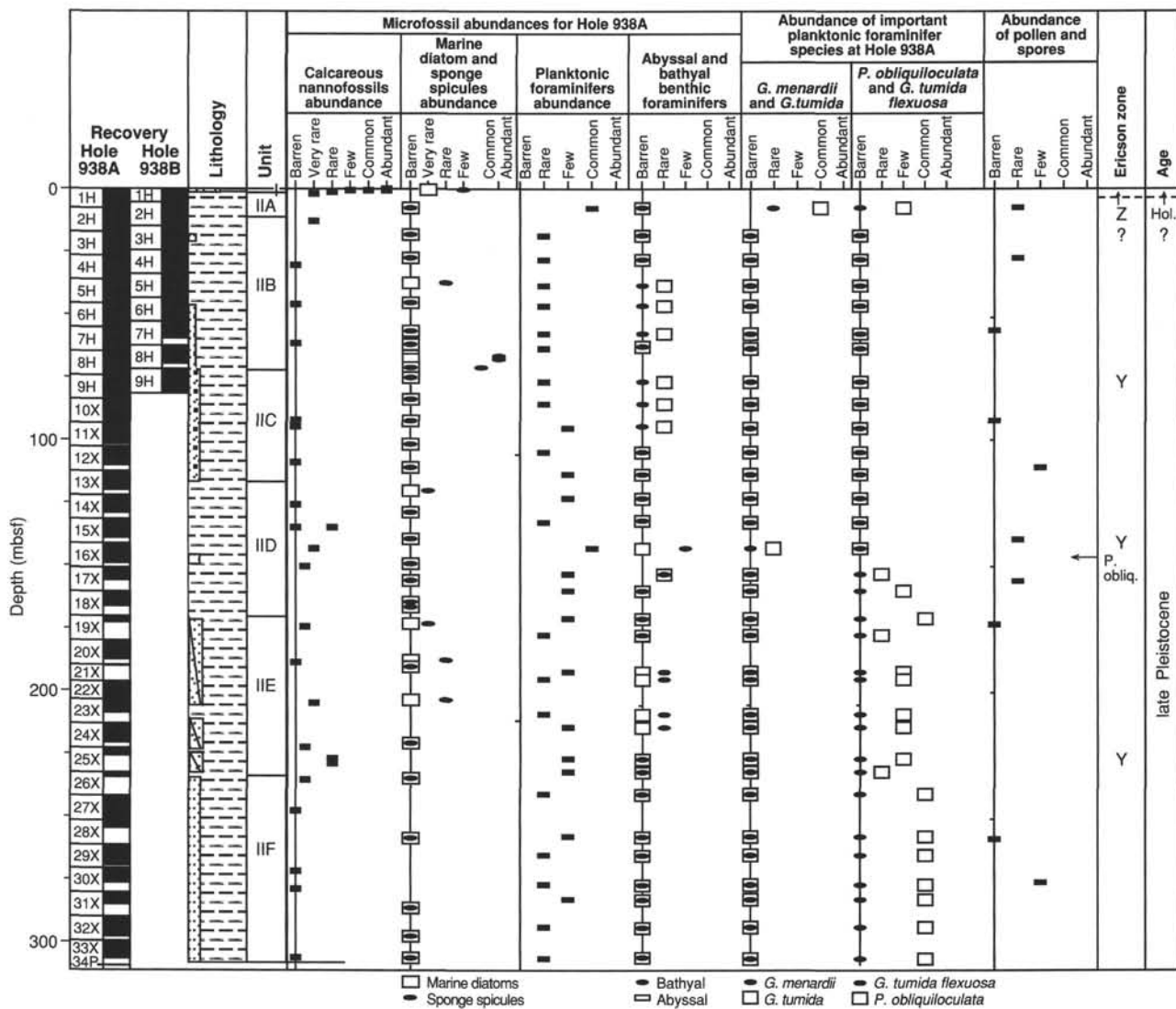


Figure 10. Biostratigraphic summary for Site 938.

4H-CC, 38–47 cm, through 10X-CC, 12–21 cm). Bathyal benthic foraminifers occur in low abundances in the lower part of Subunits IID and IIE (Samples 938A-15X-CC, 40–49 cm [138.9 mbsf], through -22X-CC, 7–16 cm [208.5 mbsf]). Bathyal foraminifers occur in intervals that contain wood, mica, and iron-stained foraminifers, suggesting a reworked component. Benthic foraminifers are absent between 220.7 mbsf and 306.3 mbsf (Samples 938A-24X-CC, 12–21 cm, through -33X-CC, 12–21 cm).

Siliceous Microfossils

Site 938 is barren of diatoms, except for the mud-line sample where a few marine species are present (e.g., *Nitzschia marina* and *Coscinodiscus nodulifer*; Table 4). The absence of solution-prone diatom species is probably the result of silica dissolution. Partially dissolved siliceous sponge spicules are present in low abundances throughout Holes 938A and 938B. Well-preserved siliceous sponge spicules occur, however, in greater quantities in discrete pellets within the Unit II (e.g., Sample 938A-8H-3, 22 cm). These pellets may represent fecal pellets, which have preserved the spicules from dissolution.

Palynology

Eight samples were examined from Hole 938A (Table 5). In general, low abundances and moderate preservation are characteristic. The late Pleistocene (Y Zone) pollen and spore assemblage has very low abundance with Cyperaceae, Rhizophoraceae, monosulcus (probably *Palmae*) pollen type, and Cyatheaceae and monolet spores present. Dinoflagellates are rare in the upper two samples (938A-1H-CC, 18–19 cm, and -3H-CC, 29–30 cm) and are not found in the other samples. Wood particles were observed in all pollen slides in low abundance. Macroscopic (>63 μm) organic material was observed in Pleistocene core-catcher samples between 110.40 mbsf and 208.37 mbsf (Table 4).

Stratigraphic Summary

Unit I contains nannofossil and planktonic foraminifer assemblages indicative of the Holocene. The nannofossil assemblages are well preserved and represent nannofossil Zone CN15b. All of Unit II between the Z/Y boundary and 306 mbsf has been defined as the Y Zone (younger than 85 ka) on the basis of the absence of *G. menardii*

Table 5. Spores and pollen data for Hole 938A.

Core, section, interval (cm)	Top interval (mbsf)	Bottom interval (mbsf)	Pollen and spores				Wood/ carbonized particles	Ericson Zone (inferred from forams.)	Age (inferred from forams.)
			Abundance	Preservation	Major types recorded	Dinocysts			
155-938A-									
1H-CC, 18-19	7.59	7.60	r	m	Trilete (verrucate) spore	r	f	Y	late Pleist.
3H-CC, 29-30	27.27	27.28	r	p	Monolete (psilate) spore	r	f	Y	late Pleist.
6H-CC, 61-62	56.32	56.33	b			b	r	Y	late Pleist.
10X-CC, 21-22	92.34	92.35	b			b	r	Y	late Pleist.
12X-CC, 22-23	110.49	110.50	f	m	Palmae, Cyatheaceae	b	f	Y	late Pleist.
15X-CC, 49-50	139.03	139.04	r	p	Cyatheaceae	b	r	Y	late Pleist.
17X-CC, 22-23	155.87	155.88	r	m	Monolete (psilate) spore	b	r	Y _{P.obliq.}	late Pleist.
19X-CC, 20-21	172.79	172.80	b			b	f	Y	late Pleist.
28X-CC, 39-40	258.29	258.30	b			b	f	Y	late Pleist.
30X-CC, 30-31	275.40	275.41	f		Rhizophoraceae, Cyperaceae	b	f	Y	late Pleist.

and *G. tumida* (Table 4). The Y_{P.obliq.} datum is at 149 mbsf in Subunit IID, suggesting that sediment below this level is older than 40 ka.

PALEOMAGNETISM
Remanence Studies

Measurements on the archive halves of all 18 APC cores and on 22 of 24 XCB cores were made using the pass-through cryogenic magnetometer. The Tensor tool provided azimuthal orientations for Cores 938A-3H through -9H. Inclinations continued to be centered on 0° for the APC cores, but were biased toward positive values for the XCB cores.

Figure 11 shows variations in inclination for the top 50 m of Hole 938A. From 15 to 46 mbsf, five oscillations in inclination are observed, beginning from high negative values and moving progressively toward more positive values. A similar pattern of oscillations was recorded in Holes 937B (24 to 27.5 mbsf in Fig. 17 of "Paleomagnetism" section, "Site 937" chapter, this volume) and 930C (64.5 to 72.5 mbsf in Fig. 20 of "Paleomagnetism" section, "Site 930" chapter, this volume). In Hole 938A, these inclination oscillations extend up to the crest of the Blue Channel levee at 20 mbsf (see Fig. 22

of "Core-Seismic Integration" section, this chapter). This distinctive trend in inclination cycles may also represent the final phase of Blue Channel deposition at Sites 930 and 937.

Sixteen oscillations in corrected declination are observed between 70 and 78 mbsf in Hole 938A (Fig. 12).

An apparent geomagnetic excursion was recorded in Sections 938A-16X-3 and -4 (144.4 to 146.0 mbsf), which is characterized by a change from high positive to moderate negative inclinations. At previous sites we have associated this characteristic inclination change with the Lake Mungo Excursion (~30 ka). This record occurs in an XCB core where AF demagnetization to 20 mT had fortunately removed much of the drill stem overprint, as indicated by resulting inclination values centered on 0°. Thirteen discrete samples from the excursion interval were AF demagnetized to 40 mT. The resulting inclinations and declinations confirmed that the excursion pattern was similar to that observed at the previous sites.

Remanence intensity variations for Holes 938A and 938B are shown in Figure 13, and the position of the apparent geomagnetic excursion with respect to the preceding intensity low (L) is identified. We have also tentatively identified five (A-E) remanence intensity peaks that appear to conform to peaks identified in previous sites at

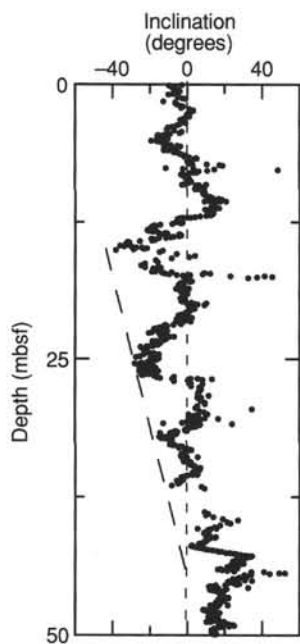


Figure 11. Inclinations of archive-half APC cores from a 50-m interval of Hole 938A. Dashed line delineates characteristic oscillatory pattern with increasingly negative inclinations. AF demagnetization level was 20 mT.

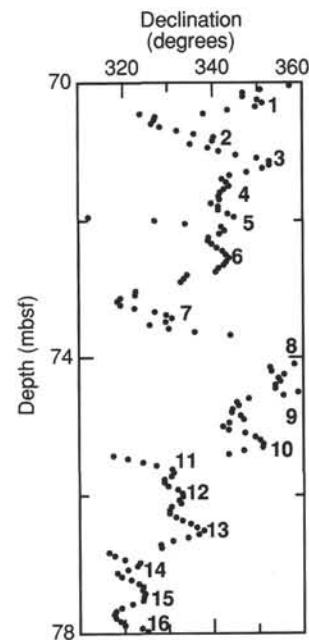


Figure 12. Azimuthally corrected declinations from an 8-m interval within archive-half APC Cores 155-938A-8H and -9H. Individual oscillations, which may correspond to secular variation, are numbered 1 through 16. AF demagnetization level was 20 mT.

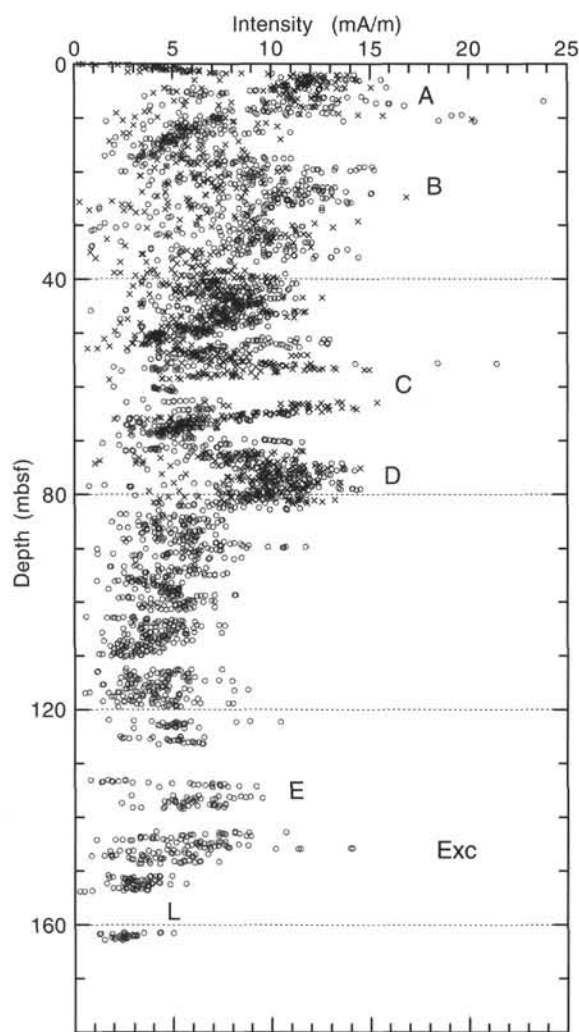


Figure 13. Remanence intensities, after AF demagnetization to 20 mT, for all measured archive-half cores from Holes 938A (circles) and 938B (x's). "Exc" marks position of apparent geomagnetic excursion (Lake Mungo at ~30 ka). A through E are characteristic intensity peaks, which may correspond to peaks identified at previous sites. Underlying intensity low is labeled as L.

approximately these same stratigraphic positions (see Fig. 15 of "Paleomagnetism" section, "Site 933" chapter, this volume).

Magnetic Susceptibility

Whole-core and discrete-sample magnetic susceptibilities were measured on all cores from this site. The results from Hole 938A are used to represent the site (Fig. 14). Both discrete-sample and whole-core data show similar downhole trends.

The highest susceptibility values are seen in Subunit IIC and probably reflect the higher silt content in this subunit. The lowest susceptibility values are within Unit I.

ORGANIC GEOCHEMISTRY

Volatile Hydrocarbons

Headspace methane concentrations in Hole 938A are moderately high throughout the core. The concentrations range from 4,250 ppm

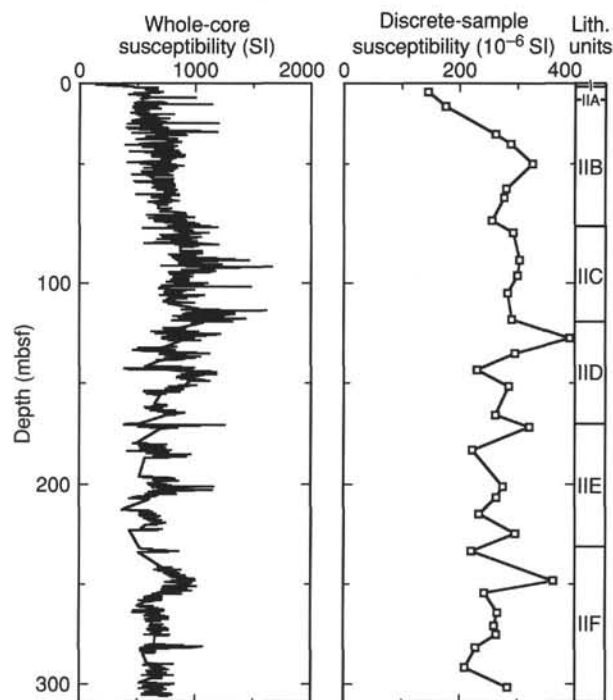


Figure 14. Whole-core and discrete-sample magnetic susceptibilities for Hole 938A.

(23.10 mbsf) to 15,500 ppm (126.50 mbsf) with a mean of about 9,000 ppm (Table 6; Fig. 15). Vacutainer methane values are higher than headspace concentrations (Fig. 15), ranging from 38,500 ppm to 633,500 ppm. Higher molecular weight hydrocarbons were not detected, indicating a predominantly biogenic methane source at Site 938.

Carbon, Nitrogen, and Sulfur Concentrations

The carbonate, calculated as CaCO_3 , content decreases from 33.4% at 0.08 mbsf to 1.5% at 4.9 mbsf and then ranges mainly from 1% to ~5% downhole (Table 7; Fig. 16). Higher concentrations are observed in light-colored bioturbated intervals at 127.17 mbsf (19%), 133.40 (7%), and 142.73 mbsf (8%). TOC is low (~0.5%) in the shallowest sample (0.08 mbsf) and then varies downhole mainly between 0.8% and 1.1%. A few lower concentrations (<0.6%) are observed in silt and sand layers (24.01, 182.55, 201.33, and 256.43 mbsf).

In general, the TN concentrations show a similar profile to that of TOC, with lower values in silt and sand layers. Most TN concentrations in Hole 938A range from 0.07% to 0.12% with high values (0.10% to 0.13%) observed between 75.61 and 127.17 mbsf. [C/N] ratios are uniform and range from 8 to 13.

In Hole 938A, total sulfur concentrations are low and generally range between 0% and 0.3%. A few higher concentrations (2% and 1.1%) are observed at the top of lithologic Unit II (4.90 and 9.46 mbsf) and at 77.69 mbsf (0.9%). As at other sites, high sulfur values are observed below the carbonate-rich Unit I.

Bitumen Characterization

Two samples (75.61 and 127.17 mbsf) were extracted with *n*-hexane for preliminary characterization of the extractable organic matter by gas chromatography. The shallower sample has an elemental composition (2.6% carbonate, 1.05% TOC) typical of lithologic Unit II. The deeper sample has a high carbonate concentration (18.9%) and a relatively high TOC concentration (0.77%). The gas chromatograms of both samples have *n*-alkane distribution patterns dominated by

Table 6. Gas concentrations in sediments from Site 938.

Core, section, interval (cm)	Depth (mbsf)	Sed. temp.* (°C)	Methane	
			HS (ppm)	VAC (ppm)
155-938A-				
1H-5, 0-5	6.00	2	9,847	
2H-6, 0-5	15.10	2	9,256	261,057
3H-5, 0-5	23.10	3	4,256	179,369
4H-6, 0-5	33.01	3	7,050	633,510
5H-6, 0-5	43.40	3	7,268	47,330
6H-7, 0-5	53.34	4	7,775	105,723
7H-4, 0-5	58.50	4	8,425	
8H-6, 0-5	71.95	4	10,974	
9H-3, 0-5	76.83	4	8,034	477,836
10X-6, 0-5	90.04	5	8,742	38,506
11X-5, 0-5	99.10	5	7,639	122,518
12X-5, 0-5	108.70	5	9,863	66,979
13X-3, 0-5	115.40	6	5,739	
14X-4, 0-5	126.50	6	15,539	
15X-3, 0-5	134.46	6	16,076	
16X-3, 0-5	144.20	7	8,758	
17X-3, 0-5	153.80	7	13,436	
18X-3, 0-5	162.88	7	11,851	
19X-2, 0-5	171.60	7	9,260	
20X-4, 0-5	184.30	8	10,574	
21X-1, 0-5	189.50	8	6,441	
22X-4, 0-5	201.00	8	9,343	
23X-2, 0-5	205.00	9	8,211	
24X-4, 0-5	217.60	9	9,973	
25X-1, 0-5	222.80	9	9,906	
26X-2, 0-5	233.80	9	9,948	
27X-4, 0-5	246.30	10	9,774	
28X-4, 0-5	255.90	10	14,157	
29X-4, 0-5	265.50	10	8,571	
30X-4, 0-5	275.10	11	11,641	
31X-3, 0-5	283.20	11	9,804	
32X-3, 0-5	292.90	11	9,798	

Notes: HS = headspace; VAC = vacutainer. Geothermal gradient = 32°C/km. Bottom-water temperature = 2°C. *See "In-situ Temperature Measurements" section, this chapter.

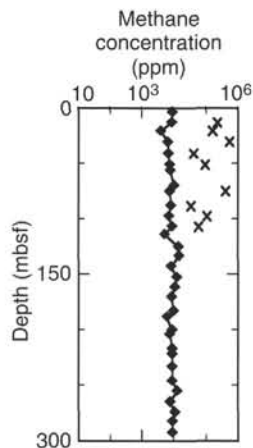


Figure 15. Methane concentrations at Site 938. Headspace (diamond) and vacutainer (x) samples are plotted.

$n\text{-C}_{29}\text{H}_{60}$ and $n\text{-C}_{31}\text{H}_{64}$, which are typical of higher land plants. This is similar to observations at previous sites.

INORGANIC GEOCHEMISTRY

Interstitial Water Analysis

Interstitial waters were collected from 14 sediment samples at Hole 938A. Samples were taken approximately every 10 m for the upper 40 mbsf and approximately every 30 m thereafter to a depth of 303.90 mbsf (Table 8; Fig. 17).

Salinities of the water samples range from 32.0 to 35.0 (Fig. 17A). From 1.45 to 42.00 mbsf, salinity decreases from 35.0 to 32.0. From

42.00 to 184.20 mbsf the salinity is constant at 32.5. Salinity increases to 34.0 at 217.50 mbsf, then decreases again to 33.0 for the remainder of the hole.

Chloride concentrations increase from 554 to 563 mM between 1.45 and 32.96 mbsf (Fig. 17B). Chlorinity is relatively constant thereafter with a slight decrease to 556 mM near the bottom of the hole (303.90 mbsf).

Pore-water pH decreases from 7.55 at 1.45 mbsf to 7.03 at 15.05 mbsf (Fig. 17C). The values increase to 7.48 at 32.96 mbsf, and then generally maintain values of 7.4–7.5 for the remainder of the hole.

Alkalinity values are more uniform than for previous sites. A slight local maximum of 13.24 mM is observed at 15.05 mbsf. Alkalinity values then increase slowly from 9.52 mM at 23.05 mbsf to 15.37 mM at 284.60 mbsf (Fig. 17D). A decrease to 11.44 mM occurs at 303.90 mbsf, near the bottom of the hole.

Magnesium and calcium profiles are once again similar to those at all previous sites. From 48.1 mM magnesium and 9.5 mM calcium at 1.45 mbsf, the concentrations decrease to around 40 mM and 5 mM, respectively, by 15.05 mbsf (Fig. 17E and 17F), and are fairly constant downhole.

Pore-water sulfate concentrations decrease from seawater values to 21.5 mM by 1.45 mbsf and to zero by 15.05 mbsf (Fig. 17G). The values remain at or near zero for most of the remainder of the hole. Several non-zero values were also measured: 1.5 mM at 126.40 and 153.70 mbsf, and 5.0 mM at 303.90 mbsf. These values are difficult to reconcile with the highly reducing conditions and probably represent a sampling artifact.

Ammonium concentrations increase with depth over the entire hole (Fig. 17H). The concentration increases rapidly over the upper 23.05 mbsf to 5.2 mM, and then more slowly downhole, to around 9 mM near the bottom of the hole.

Pore-water phosphate concentrations are 25.5 μM at 1.45 mbsf (Fig. 17I). The concentration decreases to 1.0 μM by 42.00 mbsf, and then increases gradually downhole to 12.8 μM at 303.90 mbsf.

Dissolved silica concentrations increase from 238 μM at 1.45 mbsf to 449 μM by 99.00 mbsf (Fig. 17J). Thereafter, concentrations vary between 413 and 517 μM .

Pore-water potassium concentrations decrease over the upper 15 m of the hole, from 11.9 mM at 1.45 mbsf to 9 mM at 15.05 mbsf (Fig. 17K). Below 15.05 mbsf, the values decrease more slowly, reaching a minimum of 6.7 mM at 303.90 mbsf.

Dissolved sodium concentrations decrease from 478 mM at 1.45 mbsf to 467 mM at 32.96 mbsf. Thereafter, the values vary between 468 and 475 mM downhole.

Dissolved iron at this site is high compared to iron at most previous sites. Concentrations are between 56.0 and 94.2 μM in the upper 32.96 mbsf and reach a sharp maximum of 326.4 μM at 42.00 mbsf. Values then decrease to 142.9 μM by 72.93 mbsf (Fig. 17M), and to 47.0 μM by 184.20 mbsf. Concentrations then increase slightly for the remainder of the hole to a value of 91.3 μM by 303.90 mbsf.

Manganese concentrations are at a maximum of 40.0 μM at 1.45 mbsf (Fig. 17N). Concentrations decrease to 4.0 μM by 15.05 mbsf, show a slight local maximum of 13.2 μM at 42.00 mbsf, and are relatively constant at 3.2–4.4 μM through the remainder of the hole.

A weakly cemented nodule of diagenetic siderite (FeCO_3 , determined by X-ray diffraction analysis) was recovered from sediment at a depth of 153.11 mbsf (938A-17X-2, 81–87 cm).

Sediment Geochemistry

Seven mud samples from the Blue and Channel 6 levees of the Upper Levee Complex were analyzed for major- and trace-element geochemistry (Tables 9 and 10). The compositions are uniform throughout the core, and within the range of compositions for previous sites. SiO_2 abundances vary from 62 to 64 wt%, and Al_2O_3 is between 21 and 22 wt%. CaO abundances are uniform between 0.7 and 0.9 wt%.

Table 7. Elemental and organic carbon compositions of sediments from Site 938.

Core, section, interval (cm)	Depth (mbsf)	IC (%)	CaCO ₃ * (%)	TC (%)	TOC (%)	TN (%)	TS (%)	[C/N]a	Lith. unit
155-938A-1H-1, 8-9	0.08	4.01	33.4	4.53	0.52	0.07	0.19	8	I
1H-4, 40-41	4.90	0.18	1.5	1.15	0.97	0.10	2.01	11	
2H-2, 36-37	9.46	0.61	5.1	1.31	0.70	0.08	1.09	10	
2H-4, 78-79	12.88	0.27	2.2	1.26	0.99	0.10	0.19	11	
3H-4, 57-58	22.17	0.30	2.5	1.18	0.88	0.11	0.08	10	
3H-5, 91-92	24.01	0.12	1.0	0.60	0.48	0.07	0.24	8	
4H-4, 117-118	31.18	0.22	1.8	1.13	0.91	0.10	0.11	11	
5H-4, 45-46	40.85	0.22	1.8	1.08	0.86	0.10	0.04	10	
6H-4, 78-79	49.62	0.19	1.6	1.03	0.84	0.11	0.14	9	
6H-4, 134-135	50.18	0.19	1.6	1.05	0.86	0.11	0.04	9	
7H-4, 53-54	59.03	0.24	2.0	1.12	0.88	0.10	0.05	10	
7H-5, 84-85	60.84	0.40	3.3	1.35	0.95	0.11	0.04	10	
8H-5, 29-30	70.74	0.17	1.4	1.08	0.91	0.11	0.00	10	
8H-5, 58-59	71.03	0.22	1.8	1.18	0.96	0.09	0.01	13	
9H-2, 19-20	75.61	0.31	2.6	1.36	1.05	0.12	0.02	10	
9H-3, 86-87	77.69	0.35	2.9	1.37	1.02	0.12	0.04	10	
9H-7, 31-32	81.94	0.38	3.2	1.32	0.94	0.11	0.03	10	
10X-2, 19-20	85.29	0.49	4.1	1.31	0.82	0.11	0.05	8	
10X-4, 15-16	87.42	0.28	2.3	1.15	0.87	0.11	0.15	10	
11X-4, 27-28	97.87	0.27	2.2	1.24	0.97	0.11	0.05	10	
11X-4, 106-107	98.66	0.33	2.7	1.15	0.82	0.11	0.04	10	
11X-5, 109-110	100.19	0.49	4.1	1.41	0.92	0.11	0.04	10	
12X-4, 85-86	108.05	0.34	2.8	1.28	0.94	0.13	0.04	9	
12X-5, 35-36	109.05	0.32	2.7	1.33	1.01	0.11	0.03	11	
13X-2, 91-92	114.81	0.31	2.6	1.26	0.95	0.11	0.00	10	
13X-5, 48-49	118.88	0.30	2.5	1.05	0.75	0.09	0.02	9	
13X-5, 105-106	119.45	0.33	2.7	1.18	0.85	0.11	0.12	9	
14X-1, 127-128	123.27	0.27	2.2	1.21	0.94	0.12	0.04	10	
14X-4, 67-68	127.17	2.27	18.9	3.04	0.77	0.12	0.00	7	
15X-1, 39-40	131.99	0.30	2.5	1.29	0.99	0.10	0.21	11	
15X-1, 54-55	132.14	0.31	2.6	1.27	0.96	0.10	0.13	11	
15X-2, 30-31	133.40	0.83	6.9	1.59	0.76	0.10	0.09	8	
16X-2, 3-4	142.73	0.92	7.7	1.59	0.67	0.10	0.18	8	
16X-5, 54-55	147.74	0.23	1.9	1.13	0.90	0.09	0.08	12	II
17X-2, 32-33	152.62	0.50	4.2	1.42	0.92	0.10	0.04	11	
18X-2, 110-111	162.48	0.37	3.1	1.45	1.08	0.11	0.05	11	
19X-1, 112-113	171.22	0.23	1.9	1.13	0.90	0.08	0.06	13	
20X-2, 125-126	182.55	0.17	1.4	0.51	0.34	0.04	0.04	9	
20X-4, 74-75	185.04	0.33	2.7	1.36	1.03	0.12	0.13	10	
22X-4, 30-31	201.30	0.24	2.0	0.71	0.47	0.07	0.04	8	
22X-4, 86-87	201.86	0.31	2.6	1.30	0.99	0.12	0.07	10	
23X-2, 45-46	205.45	0.32	2.7	1.36	1.04	0.11	0.05	11	
24X-4, 59-60	218.19	0.36	3.0	1.39	1.03	0.11	0.06	11	
25X-2, 104-105	224.41	0.31	2.6	1.25	0.94	0.11	0.05	10	
26X-2, 6-7	233.86	0.39	3.2	1.43	1.04	0.11	0.06	11	
27X-4, 45-47	246.75	0.28	2.3	1.20	0.92	0.10	0.03	11	
27X-6, 49-50	249.79	0.27	2.2	1.12	0.85	0.11	0.04	9	
28X-4, 53-54	256.43	0.37	3.1	0.96	0.59	0.06	0.15	11	
28X-4, 57-58	256.47	0.36	3.0	1.35	0.99	0.10	0.10	11	
29X-3, 114-115	265.14	0.45	3.7	1.32	0.87	0.10	0.05	10	
29X-6, 50-51	269.00	0.56	4.7	1.38	0.82	0.11	0.06	9	
30X-1, 34-35	270.94	0.31	2.6	1.23	0.92	0.10	0.00	11	
30X-3, 88-89	274.48	0.33	2.7	1.18	0.85	0.09	0.05	11	
31X-2, 102-103	282.72	0.58	4.8	1.44	0.86	0.10	0.00	10	
31X-3, 60-61	283.80	0.34	2.8	1.31	0.97	0.11	0.05	10	
32X-4, 93-94	295.33	0.34	2.8	1.24	0.90	0.09	0.04	11	
32X-5, 27-28	296.17	0.37	3.1	1.25	0.88	0.09	0.14	12	
33X-2, 146-147	302.46	0.55	4.6	1.39	0.84	0.10	0.00	10	
33X-3, 103-104	303.53	0.36	3.0	1.14	0.78	0.10	0.04	9	

Note: * = calculated assuming all IC is calcite.

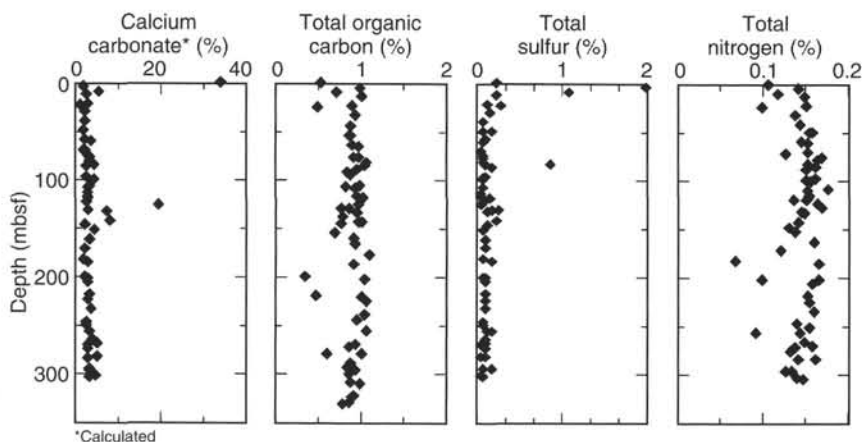


Figure 16. Concentration profiles of calcium carbonate, total organic carbon, total sulfur, and total nitrogen in Hole 938A.

Table 8. Interstitial water chemistry, Site 938.

Core, section, interval (cm)	Depth (mbsf)	Salinity	pH	Alkalinity (mM)	Cl ⁻ (mM)	Mg ²⁺ (mM)	Ca ²⁺ (mM)	K ⁺ (mM)	HPO ₄ ²⁻ (μM)	SO ₄ ²⁻ (mM)	NH ₄ ⁺ (mM)	H ₄ SiO ₄ (μM)	Na ⁺ (mM)	Fe ²⁺ (μM)	Mn ²⁺ (μM)
155-938A-															
1H-1, 145-150	1.45	35.0	7.55	9.35	554	48.1	9.5	11.9	25.5	21.5	0.9	238	478	88.4	40.0
2H-5, 145-150	15.05	34.0	7.03	13.24	560	38.8	4.8	9.0	5.1	0.2	4.2	348	473	56.0	4.0
3H-4, 145-150	23.05	32.5	7.38	9.52	561	37.3	4.2	8.6	2.1	0.4	5.2	327	474	94.2	5.2
4H-5, 145-150	32.96	33.5	7.48	8.61	563	40.1	5.2	8.7	2.1	0.2	5.5	354	467	88.5	8.4
5H-5, 145-150	42.00	32.0	7.25	10.00	563	40.4	5.6	8.3	1.0	0.2	4.8	292	468	326.4	13.2
8H-6, 98-108	72.93	32.5	7.38	8.99	563	39.2	4.2	7.7	5.0	0.3	7.2	413	471	142.9	4.4
11X-4, 140-150	99.00	32.5	7.38	10.73	563	38.0	4.8	7.5	14.0	0.7	7.3	449	475	163.3	4.4
14X-3, 140-150	126.40	32.5	7.42	9.76	562	37.7	4.7	9.9	5.2	1.5	6.4	438	474	122.8	4.4
17X-2, 140-150	153.70	32.5	7.38	9.30	563	40.1	4.6	8.2	7.5	1.5	7.7	490	470	121.4	3.2
20X-3, 140-150	184.20	32.5	7.48	11.01	562	38.2	4.2	7.5	3.1	0.5	7.6	413	474	47.0	3.6
24X-3, 140-150	217.50	34.0	7.58	12.05	559	38.6	4.4	7.0	3.4	0.5	8.2	469	471	49.0	3.8
27X-5, 140-150	249.20	33.0	7.44	13.08	562	38.2	4.4	7.5	6.6	0.3	8.8	423	474	64.3	3.6
31X-3, 140-150	284.60	33.0	7.51	15.37	557	39.2	4.8	6.8	11.8	0.4	9.1	517	469	72.6	3.8
33X-3, 140-150	303.90	33.0	7.50	11.44	556	40.4	5.2	6.7	12.8	5.0	8.2	458	471	91.3	3.4

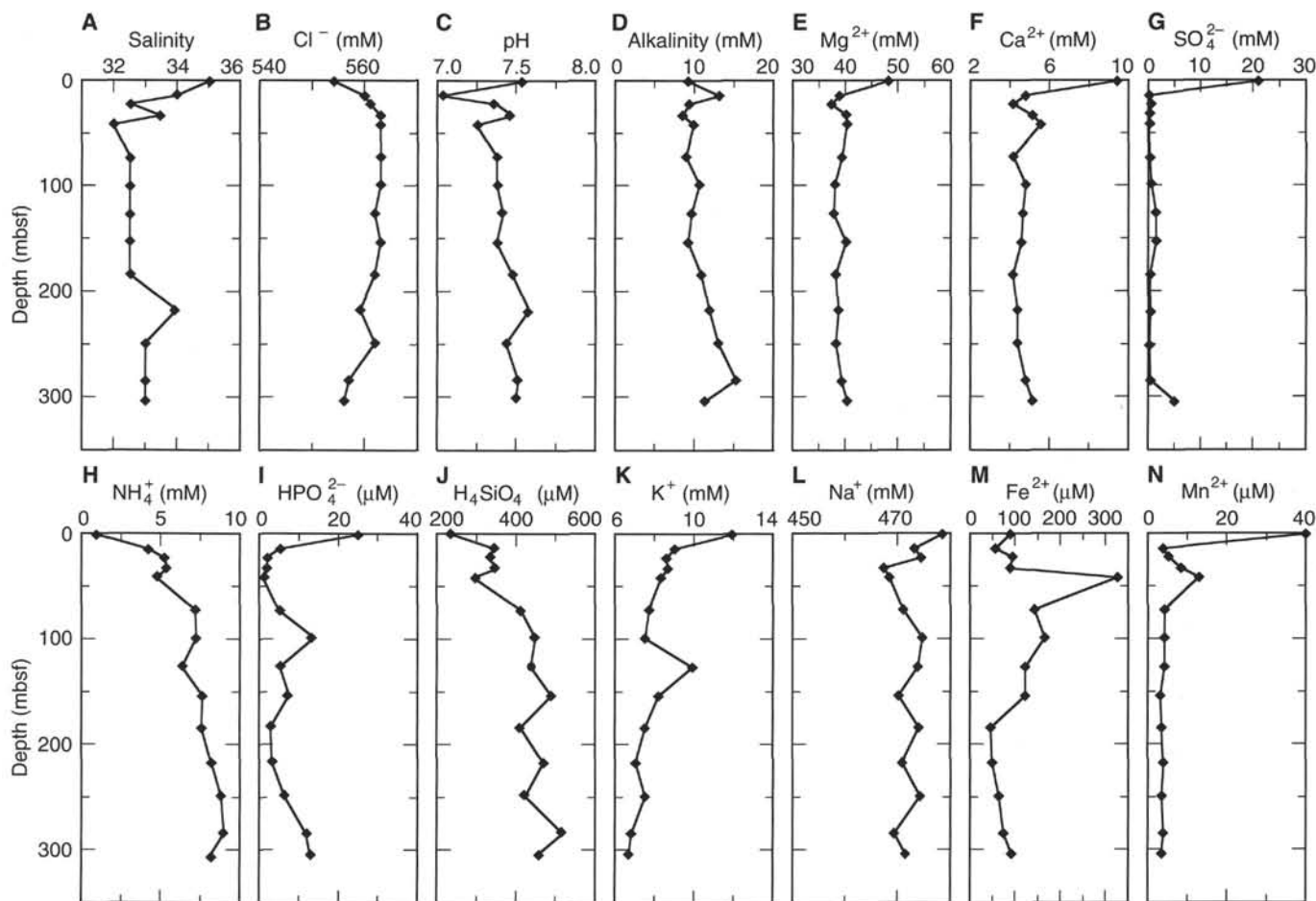


Figure 17. Downcore variation in pore-water chemistry: A. Salinity. B. Chloride. C. pH. D. Alkalinity. E. Magnesium. F. Calcium. G. Sulfate. H. Ammonium. I. Phosphate. J. Silica. K. Potassium. L. Sodium. M. Iron. N. Manganese.

PHYSICAL PROPERTIES

Index Properties

Index properties were determined only for lithologic Unit II in Hole 938A (Table 11). Within this unit, water content decreases uniformly with depth from 49% to 24% at the base of Hole 938A (Fig. 18). The corresponding downhole decrease in porosity is from 72% to 46%. Water content changes most rapidly in the uppermost part of

Unit II with values decreasing from 49% at 1.89 mbsf to 33% at 34.79 mbsf. Below this level, water content increases slightly to 34% at 32.02 mbsf before decreasing overall to the base of the hole. Several XCB cores (Cores 938A-10X, -11X, and -27X; Table 11) display distinct 3% to 4% downcore decreases in water content (Fig. 18). This pattern has been observed at previous Amazon Fan sites, most notably Sites 932 and 937, and is attributed to sediment expansion in the core barrel during coring. Below 77 mbsf, the water content profile has three slight changes in trend (Fig. 18), at about 77, 125, and 240

Table 9. Major element composition (wt%) of sediment samples, Site 938.

Core, section, interval (cm)	Depth (mbsf)	Lithology	SiO ₂	TiO ₂	Al ₂ O ₃	Fe ₂ O ₃	MnO	MgO	CaO	Na ₂ O	K ₂ O	P ₂ O ₅	Total	LOI
155-938A-														
6H-4, 135-140	50.19	Mud	62.10	1.04	21.68	7.90	0.11	2.14	0.70	1.41	3.17	0.19	100.43	7.39
9H-2, 20-24	75.62	Mud	62.57	1.10	21.53	7.70	0.11	2.09	0.81	1.51	2.99	0.21	100.64	7.92
11X-4, 29-34	97.89	Mud	62.63	1.05	21.29	7.52	0.11	2.04	0.85	1.59	2.92	0.18	100.18	7.61
13X-5, 49-54	118.89	Mud	63.13	1.08	21.47	7.80	0.10	2.01	0.82	1.41	2.99	0.16	100.96	7.90
15X-1, 40-50	132.00	Mud	61.80	1.07	21.81	7.79	0.12	2.06	0.76	1.56	3.01	0.17	100.15	7.96
28X-2, 50-55	253.40	Mud	62.22	1.08	21.12	7.72	0.10	2.04	0.77	1.41	2.90	0.18	99.54	7.60
32X-5, 28-33	296.18	Mud	63.52	1.06	20.58	7.23	0.10	1.95	0.80	1.60	2.91	0.16	99.90	7.05

Notes: Total iron is reported as Fe₂O₃. LOI = loss on ignition.

Table 10. Trace element composition (ppm) of sediment samples, Site 938.

Core, section, interval (cm)	Depth (mbsf)	Lithology	Ba	Ce	Cr	Cu	Nb	Ni	Rb	Sr	V	Y	Zn	Zr
155-938A-														
6H-4, 135-140	50.19	Mud	505	112	68	33	22	34	138	145	88	37	127	222
9H-2, 20-24	75.62	Mud	487	109	65	31	22	32	131	149	82	40	125	237
11X-4, 29-34	97.89	Mud	488	106	63	32	21	32	127	152	86	40	124	235
13X-5, 49-54	118.89	Mud	485	102	65	32	20	31	128	149	82	38	124	234
15X-1, 40-50	132.00	Mud	484	105	69	34	22	34	130	145	84	39	128	230
28X-2, 50-55	253.40	Mud	488	104	66	31	22	33	128	148	90	41	126	249
32X-5, 28-33	296.18	Mud	480	99	67	29	22	32	127	151	85	41	120	259

mbsf. These changes are possibly related to changes in sedimentation rate.

Grain density averages 2.75 g/cm³ with most of the values contained in the range of 2.7 to 2.8 g/cm³ (Table 11). Grain density decreases downhole (Fig. 18) to a minima at about 165 mbsf. The trend reverses at 165 mbsf, and grain density increases to the base of the hole. The minima corresponds to the top of the Channel 6 System (Fig. 24). The grain density changes probably result from mineralogical variations and imply changes in sediment source.

Downhole variation of wet-bulk density essentially matches the variation in water content (Fig. 18). From the top to the base of Hole 938A, wet-bulk density increases from approximately 1.5 to 2.0 g/cm³. Comparison of the discrete-sample wet-bulk densities with the GRAPE bulk density profile provides a qualitative measure of the expansion experienced by the cores. The difference between the two data sets increases over the upper 30 m from 0.1 to 0.4 g/cm³ (Fig. 18). Below 30 mbsf, the GRAPE densities remain between 0.3 and 0.4 g/cm³ less than the discrete sample values. Unlike at Sites 937 and 939, there is no overlap of discrete and GRAPE wet-bulk density profiles.

Compressional-wave Velocity

Pervasive microfractures in sediment affected by gas expansion restricted PWL measurements to the interval from 0 to 6.55 mbsf in Hole 938A and 0 to 5.07 mbsf in Hole 938B. The average transverse velocities are 1491 m/s and 1514 m/s, respectively. Longitudinal and transverse velocity measurements using the DSV were only successful in Core 938A-1H down to 5.30 mbsf. Velocities range from 1491 to 1498 m/s and show isotropic behavior and good agreement with the PWL results.

Shear Strength

Measurements of undrained shear strength were made using the motorized shear vane on all cores from Hole 938A (Table 12). Below 65 mbsf, compressive strengths were determined using a pocket penetrometer. The correlation between shear-strength values estimated from the compressive strength and those determined by the lab vane is good ($r = 0.90$); however, the regression equation ($S_u[\text{est}] = 0.79 \cdot q_u/2 + 2.73$) indicates that the penetrometer yields measurements that overestimate the lab vane values.

The strength profile for Hole 938A (Fig. 19) can be divided into two parts by a downhole increase in scatter that begins at approximately 65 mbsf. Within the upper interval, undrained shear strength increases relatively uniformly from 7 kPa just below the seafloor to 28 kPa at 65 mbsf. The trend of increasing strength with depth is interrupted by high values in the first four sections of Core 938A-5H (37 to 42 mbsf). This maxima occurs close to anomalies in index property profiles (Fig. 18) and includes a 2.5-m zone of drilling disturbed sediment at the top of Core 938A-5H. Below 65 mbsf, shear strength increases downhole, but with greater variability. An increase of about 30 kPa appears to occur between 225 and 240 mbsf. This increase approximately corresponds to the boundary between Subunits IIE and IIF at 233.73 mbsf.

In the lower part of the strength profile, shear strength increases with depth in individual cores. This pattern is well developed in Cores 938A-22X, -27X, -30X, and -32X and is generally matched by an increase in compressive strength. As with the index properties, the changes in shear and compressive strengths are attributed to expansion of the upper part and possible compression of the lower part of cores during coring.

The residual undrained shear strength also increases downhole (Table 12), but at a lower rate than the peak strength, resulting in a slight downhole decrease in the ratio of residual to peak undrained shear strength. Although individual cores show distinct downcore trends in the ratio, the trends are not as consistent as those in Hole 937B.

Resistivity

Longitudinal and transverse resistivity were determined at depths coinciding with the depths of index property measurements in Hole 938A (Table 13). The longitudinal resistivity displays a general downhole increase (Fig. 20) that parallels the downhole decrease in porosity. Resistivity increases from 0.25 Ωm near the seafloor to 0.43 Ωm at the base of Hole 938A. Comparison of longitudinal and transverse resistivities indicates slight lithologic-dependent variations in anisotropy (Fig. 20). However, the dependence is not as pronounced as that at previous sites on the Amazon Fan. The change from the clays with numerous silt laminae of Subunits IIB and IIC to the almost laminae-free Subunit IID corresponds to a change from anisotropy that is widely scattered and overwhelmingly negative (average -3.71%) to anisotropy that is more closely grouped and less negative

Table II. Index properties at Site 938.

Core, section, interval (cm)	Depth (mbsf)	Water content (%)	Wet-bulk density (g/cm ³)	Grain density (g/cm ³)	Dry-bulk density (g/cm ³)	Porosity (%)	Void ratio
155-938A-							
1H-2, 39-41	1.89	49.3	1.53	2.66	0.75	71.6	2.52
1H-3, 58-60	3.58	47.2	1.54	2.68	0.80	70.1	2.34
1H-4, 79-81	5.29	45.8	1.60	2.74	0.84	69.3	2.26
1H-5, 104-106	7.04	44.0	1.60	2.68	0.88	67.3	2.05
2H-1, 103-105	8.63	43.4	1.63	2.76	0.90	67.4	2.07
2H-2, 83-85	9.93	43.0	1.64	2.74	0.91	66.9	2.02
2H-3, 104-106	11.64	42.0	1.65	2.83	0.94	66.7	2.00
2H-4, 88-90	12.98	41.3	1.65	2.73	0.95	65.2	1.88
2H-5, 72-74	14.32	39.5	1.71	2.88	1.02	64.7	1.84
2H-6, 110-112	16.20	39.2	1.68	2.70	1.00	62.9	1.70
2H-7, 57-59	17.17	38.0	1.73	2.81	1.05	62.6	1.68
3H-1, 90-92	18.00	38.4	1.70	2.74	1.03	62.5	1.67
3H-2, 90-92	19.50	38.2	1.71	2.71	1.03	62.0	1.63
3H-3, 88-90	20.98	38.1	1.66	2.70	1.03	61.9	1.62
3H-4, 104-106	22.64	37.2	1.74	2.77	1.06	61.6	1.60
3H-5, 101-103	24.11	36.1	1.75	2.70	1.08	59.9	1.49
3H-6, 81-83	25.41	35.4	1.76	2.71	1.11	59.2	1.45
3H-7, 64-66	26.74	35.4	1.75	2.73	1.11	59.4	1.46
4H-2, 46-48	27.47	35.0	1.76	2.75	1.12	59.1	1.44
4H-3, 43-45	28.94	34.7	1.78	2.81	1.14	59.3	1.46
4H-4, 50-52	30.51	34.3	1.76	2.76	1.15	58.5	1.41
4H-5, 51-53	32.02	34.4	1.78	2.73	1.14	58.2	1.39
4H-6, 69-71	33.70	33.1	1.80	2.79	1.19	57.4	1.35
4H-7, 28-30	34.79	32.9	1.84	2.80	1.20	57.3	1.34
4H-7, 117-119	35.68	33.5	1.82	2.82	1.18	58.1	1.39
4H-8, 52-54	36.53	33.9	1.81	2.79	1.16	58.2	1.39
5H-1, 109-111	37.19	34.4	1.77	2.80	1.15	58.9	1.43
5H-2, 114-116	38.74	34.2	1.79	2.73	1.14	58.0	1.38
5H-3, 109-111	39.99	33.8	1.81	2.81	1.17	58.3	1.40
5H-4, 117-119	41.57	33.3	1.81	2.82	1.19	57.8	1.37
5H-5, 50-52	42.40	33.4	1.78	2.75	1.17	57.3	1.34
5H-6, 24-26	43.64	33.3	1.79	2.77	1.18	57.5	1.35
5H-7, 112-114	46.02	32.8	1.82	2.77	1.19	56.9	1.32
6H-2, 58-60	46.42	32.6	1.84	2.84	1.21	57.3	1.34
6H-3, 126-128	48.60	32.8	1.80	2.76	1.19	56.8	1.32
6H-4, 89-91	49.73	32.8	1.80	2.72	1.18	56.5	1.30
6H-5, 92-94	51.26	32.4	1.82	2.75	1.20	56.3	1.29
6H-6, 87-89	52.71	32.5	1.82	2.86	1.22	57.3	1.34
6H-7, 25-27	53.59	32.4	1.80	2.70	1.19	55.8	1.26
6H-8, 77-79	55.61	32.0	1.80	2.72	1.21	55.5	1.25
7H-2, 53-55	56.03	32.4	1.81	2.79	1.21	56.5	1.30
7H-3, 78-80	57.78	33.0	1.79	2.74	1.18	56.8	1.32
7H-4, 75-77	59.25	31.8	1.82	2.79	1.23	55.9	1.27
7H-5, 48-50	60.48	31.2	1.84	2.75	1.24	54.8	1.21
7H-7, 35-37	62.73	31.7	1.85	2.80	1.23	55.8	1.26
7H-8, 28-30	64.16	31.2	1.83	2.74	1.24	54.8	1.21
8H-1, 72-74	65.32	31.4	1.85	2.79	1.24	55.5	1.25
8H-2, 40-42	66.50	29.4	1.90	2.84	1.32	53.6	1.15
8H-3, 61-63	68.21	31.1	1.87	2.82	1.26	55.4	1.24
8H-4, 68-70	69.78	30.6	1.87	2.81	1.27	54.7	1.21
8H-5, 81-83	71.26	31.0	1.88	2.83	1.26	55.4	1.24
8H-6, 53-55	72.48	31.0	1.86	2.84	1.26	55.4	1.24
8H-7, 35-37	73.38	30.7	1.88	2.81	1.27	54.8	1.21
9H-1, 66-68	74.76	31.2	1.84	2.73	1.24	54.7	1.21
9H-2, 60-62	76.02	30.7	1.85	2.76	1.26	54.4	1.19
9H-3, 64-66	77.47	29.3	1.93	2.81	1.31	53.2	1.14
9H-5, 40-42	79.03	29.7	1.92	2.79	1.30	53.5	1.15
9H-6, 36-38	80.49	28.7	1.94	2.81	1.34	52.5	1.10
9H-7, 67-69	82.30	29.4	1.91	2.80	1.31	53.3	1.14
10X-1, 91-93	84.51	32.7	1.85	2.77	1.20	56.8	1.31
10X-3, 40-42	86.17	30.7	1.86	2.77	1.26	54.5	1.20
10X-4, 46-48	87.73	30.2	1.86	2.71	1.27	53.4	1.14
10X-5, 42-44	89.19	30.7	1.86	2.72	1.25	54.1	1.18
10X-6, 38-40	90.42	29.3	1.91	2.74	1.30	52.5	1.11
10X-7, 28-30	91.82	28.7	1.91	2.78	1.33	52.2	1.09
11X-1, 61-63	93.71	33.2	1.82	2.76	1.18	57.2	1.34
11X-2, 61-63	95.21	30.8	1.87	2.72	1.25	54.1	1.18
11X-3, 53-55	96.63	29.8	1.87	2.73	1.28	53.1	1.13
11X-4, 54-56	98.14	29.9	1.90	2.75	1.28	53.4	1.14
11X-5, 64-66	99.74	30.7	1.89	2.76	1.26	54.3	1.19
11X-6, 57-59	101.17	28.4	1.92	2.77	1.33	51.8	1.07
12X-1, 62-64	103.32	31.0	1.86	2.69	1.23	54.2	1.18
12X-2, 62-64	104.82	30.4	1.85	2.73	1.26	53.7	1.16
12X-3, 62-64	106.32	33.0	1.82	2.77	1.19	57.1	1.33
12X-4, 62-64	107.82	31.3	1.89	2.78	1.24	55.3	1.23
12X-5, 62-64	109.32	31.4	1.87	2.78	1.24	55.4	1.24
13X-1, 59-61	112.99	31.4	1.84	2.70	1.22	54.7	1.21
13X-2, 59-61	114.49	27.9	1.93	2.75	1.35	50.9	1.04
13X-3, 59-61	115.99	30.9	1.87	2.74	1.25	54.5	1.20
13X-4, 59-61	117.49	24.7	1.98	2.73	1.46	46.7	0.87
13X-5, 59-61	118.99	29.7	1.91	2.76	1.29	53.2	1.14
14X-1, 59-61	122.59	31.9	1.86	2.76	1.22	55.8	1.26
14X-2, 59-61	124.09	31.9	1.81	2.72	1.21	55.5	1.25
14X-3, 59-61	125.59	32.1	1.83	2.72	1.21	55.6	1.25
14X-4, 59-61	127.09	31.3	1.85	2.70	1.23	54.6	1.20
14X-5, 34-36	128.34	30.4	1.87	2.75	1.27	54.0	1.17
15X-1, 89-91	132.49	31.9	1.84	2.71	1.21	55.3	1.24

Table 11 (continued).

Core, section, interval (cm)	Depth (mbsf)	Water content (%)	Wet-bulk density (g/cm ³)	Grain density (g/cm ³)	Dry-bulk density (g/cm ³)	Porosity (%)	Void ratio
15X-2, 89-91	133.99	31.5	1.84	2.73	1.22	55.1	1.23
15X-3, 89-91	135.35	29.9	1.89	2.75	1.28	53.4	1.14
15X-4, 89-91	136.85	29.9	1.87	2.71	1.27	53.0	1.13
15X-5, 89-91	138.35	30.3	1.89	2.73	1.26	53.7	1.16
16X-1, 80-82	142.00	29.2	1.87	2.72	1.30	52.3	1.10
16X-2, 81-83	143.51	29.4	1.90	2.72	1.29	52.5	1.11
16X-3, 81-83	145.01	27.7	1.92	2.71	1.35	50.3	1.01
16X-4, 76-78	146.46	30.3	1.88	2.70	1.26	53.4	1.14
16X-5, 76-78	147.96	29.1	1.92	2.76	1.31	52.5	1.11
17X-1, 104-106	151.84	29.3	1.89	2.68	1.29	52.0	1.08
17X-2, 104-106	153.34	29.5	1.88	2.68	1.28	52.2	1.09
17X-3, 106-108	154.86	30.3	1.88	2.74	1.27	53.7	1.16
18X-2, 9-11	161.47	29.4	1.87	2.69	1.29	52.3	1.10
18X-3, 59-61	163.47	28.9	1.90	2.73	1.31	51.9	1.08
18X-4, 92-94	165.30	27.7	1.93	2.67	1.34	50.1	1.00
19X-1, 73-75	170.83	30.5	1.85	2.73	1.26	53.9	1.17
19X-2, 73-75	172.33	30.5	1.88	2.74	1.26	54.0	1.17
19X-CC, 3-5	172.62	28.3	1.96	2.82	1.35	52.1	1.09
20X-1, 72-74	180.52	30.0	1.86	2.71	1.27	53.1	1.13
20X-2, 65-67	181.95	28.5	1.89	2.72	1.32	51.5	1.06
20X-3, 75-77	183.55	28.0	1.92	2.71	1.33	50.7	1.03
20X-4, 88-90	185.18	28.7	1.89	2.69	1.31	51.4	1.06
20X-5, 86-88	186.66	28.3	1.90	2.73	1.33	51.2	1.05
22X-1, 114-116	197.64	28.8	1.89	2.70	1.31	51.6	1.07
22X-2, 94-96	198.94	28.1	1.90	2.68	1.32	50.6	1.03
22X-3, 104-106	200.54	27.8	1.92	2.71	1.34	50.5	1.02
22X-4, 97-99	201.97	28.0	1.94	2.73	1.34	50.9	1.04
22X-5, 61-63	203.11	27.3	1.92	2.72	1.36	49.9	0.99
23X-1, 75-77	204.25	28.9	1.90	2.74	1.31	52.1	1.09
23X-2, 84-86	205.84	28.5	1.90	2.68	1.31	51.0	1.04
23X-CC, 51-53	208.25	27.3	1.95	2.75	1.37	50.2	1.01
24X-1, 84-86	213.94	28.8	1.89	2.68	1.30	51.5	1.06
24X-2, 84-86	215.44	28.9	1.91	2.75	1.32	52.2	1.09
24X-3, 84-86	216.94	27.5	1.92	2.73	1.36	50.3	1.01
24X-4, 84-86	218.44	26.8	1.92	2.72	1.38	49.4	0.97
24X-5, 84-86	219.94	27.4	1.93	2.70	1.35	49.9	1.00
25X-1, 34-36	223.14	27.5	1.92	2.70	1.35	50.0	1.00
25X-2, 36-38	223.73	24.7	1.99	2.67	1.44	46.1	0.86
25X-CC, 35-37	225.22	26.9	1.97	2.83	1.40	50.5	1.02
26X-1, 125-127	233.55	25.0	2.01	2.77	1.46	47.3	0.90
26X-2, 25-27	234.05	26.2	1.95	2.71	1.40	48.5	0.94
27X-1, 109-111	242.89	26.3	1.96	2.75	1.41	48.9	0.96
27X-2, 106-108	244.36	26.2	1.98	2.75	1.41	48.9	0.96
27X-3, 94-96	245.74	25.3	2.00	2.81	1.46	48.1	0.93
27X-4, 110-112	247.40	24.3	1.98	2.73	1.47	46.1	0.85
27X-5, 62-64	248.42	23.7	2.03	2.77	1.50	45.7	0.84
27X-6, 114-116	250.44	24.5	2.00	2.80	1.49	47.0	0.89
28X-1, 104-106	252.44	25.7	1.95	2.73	1.42	48.0	0.92
28X-2, 104-106	253.94	26.3	1.95	2.73	1.40	48.8	0.95
28X-3, 104-106	255.44	26.1	1.95	2.75	1.41	48.7	0.95
28X-4, 104-106	256.94	26.3	1.95	2.77	1.41	49.1	0.96
28X-5, 104-106	258.44	25.3	1.96	2.73	1.44	47.4	0.90
29X-1, 104-106	262.04	26.6	1.95	2.72	1.39	49.1	0.97
29X-2, 104-106	263.54	26.8	1.97	2.81	1.40	50.1	1.00
29X-3, 104-106	265.04	25.6	1.97	2.76	1.43	48.1	0.93
29X-4, 104-106	266.54	26.0	1.96	2.72	1.41	48.2	0.93
29X-5, 104-106	268.04	25.3	1.97	2.75	1.44	47.6	0.91
29X-6, 22-24	268.72	24.8	2.01	2.75	1.46	47.0	0.89
30X-1, 39-41	270.99	26.6	1.95	2.76	1.40	49.3	0.97
30X-2, 39-41	272.49	26.6	1.97	2.77	1.40	49.4	0.98
30X-3, 39-41	273.99	25.5	1.99	2.78	1.44	48.1	0.93
30X-4, 39-41	275.49	25.6	1.98	2.74	1.43	47.9	0.92
31X-1, 132-134	281.52	27.6	1.93	2.76	1.36	50.6	1.03
31X-2, 129-131	282.99	26.3	1.98	2.78	1.42	49.2	0.97
31X-3, 129-131	284.49	25.9	1.99	2.80	1.43	48.9	0.96
32X-1, 101-103	290.91	26.8	1.94	2.79	1.40	49.9	1.00
32X-2, 86-88	292.26	24.9	2.02	2.78	1.46	47.3	0.90
32X-3, 86-88	293.76	25.4	1.98	2.77	1.44	47.9	0.92
32X-4, 86-88	295.26	25.2	1.96	2.76	1.45	47.5	0.91
32X-5, 86-88	296.76	25.0	1.97	2.78	1.46	47.5	0.90
33X-1, 65-67	300.15	24.5	2.02	2.74	1.47	46.5	0.87
33X-2, 65-67	301.65	24.0	2.05	2.81	1.51	46.5	0.87
33X-3, 65-67	303.15	24.7	1.98	2.82	1.48	47.4	0.90
33X-4, 65-67	304.65	25.5	2.01	2.77	1.44	48.0	0.92
33X-5, 46-48	305.96	24.4	1.99	2.74	1.47	46.3	0.86

(average -1.58%). Similar changes occur in other Amazon Fan holes (e.g., Holes 931B and 933A). A similar reduction in average anisotropy from -2.75% in Subunit IIE to -0.92% in Subunit IIF corresponds with the decrease in laminae in Subunit IIF. Unlike the transition between Subunits IIC and IID, the scatter in anisotropy in Subunits IIE and IIF does not differ significantly.

CORE-SEISMIC INTEGRATION

Hole 938A is located on the flank of the Blue Channel-levee System and was cored to 306.35 mbsf through the Blue Channel-levee System and into the older Channel-levee System 6 of the Upper Levee Complex (Damuth et al., 1983; Manley and Flood, 1988). Six

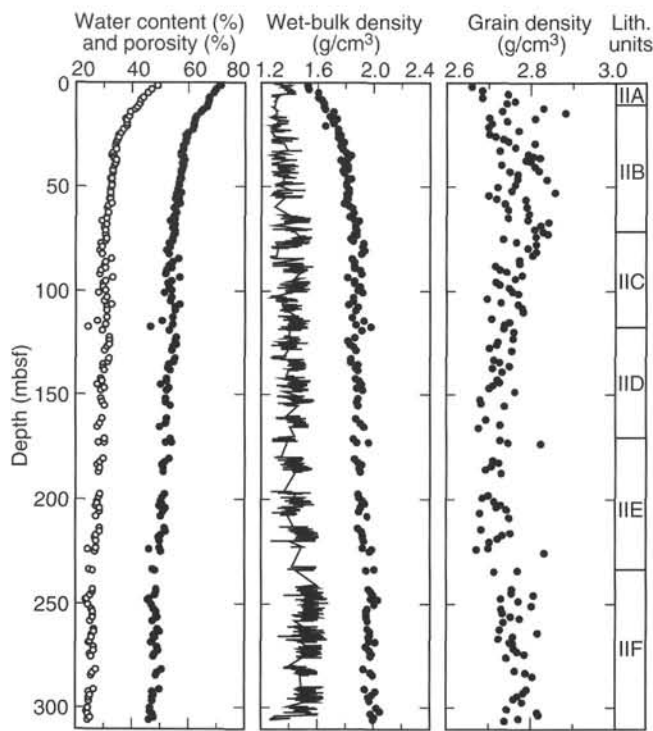


Figure 18. Water content (open circles) and porosity (solid circles), wet-bulk density as determined for discrete samples and by the GRAPE (line), and grain density derived from discrete samples.

seismic-facies units are identified on 3.5-kHz (Fig. 2) and water-gun seismic profiles (1243UTC on 27 April 1994 during Leg 155; Fig. 21). Seismic-facies Units 1 and 2 are classified using 3.5-kHz profiles, whereas Units 3 through 6 are classified from the water-gun profiles (Fig. 22). Moderate-amplitude reflections are observed at the boundaries between seismic facies at 13, 30, 160, and 215 ms.

Preliminary correlation between the seismic-facies units and the lithologic units (Fig. 22) was based on the velocity-depth equation determined at Site 931. Seismic-facies Unit 1 (0–13 ms) is acoustically transparent and encompasses all of lithologic Unit I and Subunit IIA, which is composed of mottled clay. Seismic-facies Unit 2 (13–30 ms) is characterized by low-amplitude, continuous, slightly convergent reflections. This seismic-facies unit correlates with the upper 8 m of lithologic Subunit IIB, which is composed of silty clay with laminae and beds of silt. The interface between seismic-facies Units 1 and 2 correlates approximately to the lithologic boundary between Subunits IIA and IIB at 10 mbsf and relates to the first occurrence of silt laminae observed in Subunit IIB. High-amplitude reflections observed at 25 ms and 30 ms on the 3.5-kHz profile correspond to a short interval of frequent silt laminae within Subunit IIB. Seismic-facies Units 1 and 2 appear to have been deposited when the Amazon through Purple Channel-levee systems were active.

Seismic-facies Unit 3 (30–160 ms) exhibits medium-amplitude, continuous divergent reflections from 30 to 160 ms. This unit correlates to lithologic Subunits IIB through IIC, which are composed of silty clay with thin- to medium-bedded silt and fine sand turbidites. Seismic-facies Unit 3 correlates with the Blue Channel-levee System. The top of the Blue system is uncertain, but occurs between 30 and 54 ms. A prominent reflection at 160 ms represents the boundary between the Blue Channel-levee System and the underlying Channel 5 through Yellow systems.

Seismic-facies Unit 4 has high-amplitude, continuous divergent reflections between 160 and 215 ms. These reflections dip less steeply than those of Unit 3 and correspond to most of lithologic Subunit

Table 12. Undrained shear strength at Site 938.

Core, section, interval (cm)	Depth (mbsf)	Peak undrained shear strength (kPa)	Residual undrained shear strength (kPa)	Unconfined compressive strength* (kPa)
155-938A-				
1H-1, 40	1.90	7.4	5.5	
1H-2, 60	3.60	6.5	4.5	
1H-4, 80	5.30	8.0	5.8	
1H-5, 105	7.05	7.6	5.6	
2H-1, 104	8.64	8.2	6.2	
2H-2, 84	9.94	7.6	5.0	
2H-3, 105	11.65	8.2	5.2	
2H-4, 89	12.99	10.7	7.6	
2H-5, 73	14.33	8.2	5.8	
2H-6, 111	16.21	7.2	4.7	
2H-7, 58	17.18	9.6	6.6	
3H-1, 91	18.01	15.0	10.0	
3H-2, 91	19.51	13.5	8.9	
3H-3, 89	20.99	15.6	10.0	
3H-4, 105	22.65	19.5	12.1	
3H-5, 102	24.12	14.2	9.2	
3H-6, 82	25.42	13.1	8.7	
3H-7, 64	26.74	12.8	9.3	
4H-2, 47	27.48	20.5	12.8	
4H-3, 44	28.95	17.0	11.5	
4H-4, 51	30.52	18.3	11.9	
4H-5, 52	32.03	14.5	7.9	
4H-6, 70	33.71	23.0	13.5	
4H-7, 29	34.80	16.9	7.9	
4H-7, 118	35.69	14.0	5.7	
4H-8, 53	36.54	19.2	11.3	
5H-1, 110	37.20	27.6	15.5	
5H-2, 115	38.75	34.0	18.0	
5H-3, 110	40.00	32.3	18.0	
5H-4, 118	41.58	32.2	19.6	
5H-5, 51	42.41	25.7	16.5	
5H-6, 25	43.65	20.9	13.9	
5H-7, 113	46.03	19.5	13.1	
6H-2, 59	46.43	29.7	18.7	
6H-3, 127	48.61	24.3	15.0	
6H-4, 90	49.74	22.3	12.4	
6H-5, 93	51.27	27.7	16.9	
6H-6, 88	52.72	27.4	15.7	
6H-7, 26	53.60	20.9	13.9	
6H-8, 78	55.62	26.9	17.4	
7H-2, 54	56.04	22.6	10.3	
7H-3, 79	57.79	16.4	11.8	
7H-4, 76	59.26	21.2	14.6	
7H-5, 49	60.49	21.8	15.3	
7H-7, 36	62.74	27.2	15.5	
7H-8, 29	64.17	28.0	19.1	
8H-1, 73	65.33	30.6	15.6	58.9
8H-2, 41	66.51	36.2	20.7	68.7
8H-3, 62	68.22	26.9	13.1	68.7
8H-4, 69	69.79	24.3	16.4	58.9
8H-5, 82	71.27	32.8	20.0	73.6
8H-6, 54	72.49	34.8	19.9	73.6
8H-7, 36	73.39	24.6	15.2	63.8
9H-1, 66	74.76	50.4	25.1	117.7
9H-2, 60	76.02	42.7	19.1	122.6
9H-3, 64	77.47	38.8	18.4	112.8
9H-5, 41	79.04	23.2	12.8	98.1
9H-6, 37	80.50	28.0	13.6	98.1
9H-7, 67	82.30	32.5	16.2	103.0
10X-1, 92	84.52	18.4	12.2	
10X-2, 40	85.50			63.8
10X-3, 41	86.18	20.7	14.4	
10X-4, 47	87.74	34.8	21.0	
10X-5, 43	89.20	30.0	18.1	
10X-6, 39	90.43	37.3	22.3	
11X-1, 62	93.72	18.0	14.0	
11X-2, 62	95.22	31.9	21.0	
11X-3, 55	96.65	37.0	23.5	117.7
11X-4, 55	98.15	38.6	25.3	107.9
11X-5, 65	99.75	33.4	22.8	88.3
11X-6, 58	101.18	38.1	23.8	93.2
12X-1, 63	103.33	26.7	19.1	49.1
12X-2, 63	104.83	35.0	23.6	68.7
12X-3, 63	106.33	16.5	12.0	
12X-4, 63	107.83	28.8	19.2	
12X-5, 63	109.33	40.6	25.7	93.2
13X-1, 60	113.00	24.7	17.4	88.3
13X-2, 60	114.50	35.0	23.5	63.8
13X-3, 60	116.00	40.6	25.9	107.9
13X-4, 60	117.50	37.5	25.0	68.7
13X-5, 60	119.00	40.6	26.2	122.6
14X-1, 60	122.60	26.7	19.4	88.3
14X-1, 60	124.10	34.5	23.4	93.2
14X-3, 60	125.60	37.0	23.8	88.3

Table 12 (continued).

Core, section, interval (cm)	Depth (mbsf)	Peak undrained shear strength (kPa)	Residual undrained shear strength (kPa)	Unconfined compressive strength* (kPa)
14X-4, 60	127.10	42.2	25.4	107.9
14X-5, 35	128.35	48.3	31.5	122.6
15X-1, 90	132.50	33.6	23.4	78.5
15X-2, 90	134.00	47.7	32.0	117.7
15X-2, 90	135.50	49.5	31.2	112.8
15X-4, 90	136.86	60.1	36.4	171.7
15X-5, 90	138.36	45.1	30.1	107.9
16X-1, 82	142.02	39.8	26.2	88.3
16X-2, 82	143.52	48.6	31.0	107.9
16X-3, 82	145.02	70.7	41.8	171.7
16X-4, 77	146.47	31.8	21.2	98.1
16X-5, 77	147.97	51.3	30.0	132.4
17X-1, 105	151.85	45.1	36.3	117.7
17X-2, 105	153.35	56.6	31.1	112.8
17X-3, 107	154.87	33.6	21.5	117.7
18X-2, 10	161.48	49.5	33.5	122.6
18X-3, 60	163.48	53.9	35.4	112.8
18X-4, 93	165.31	72.5	43.5	210.9
19X-1, 71	170.81	28.3	21.7	
19X-2, 74	172.34	28.3	18.6	68.7
19X-CC, 4	172.63	52.2	21.9	107.9
20X-1, 73	180.53	40.7	26.7	88.3
20X-2, 66	181.96	49.5	24.5	98.1
20X-3, 76	183.56	50.4	30.5	112.8
20X-4, 89	185.19	68.1	41.5	137.3
20X-5, 87	186.67	63.6	41.6	137.3
22X-1, 115	197.65	45.1	23.0	93.2
22X-2, 95	198.95	58.3	25.7	127.5
22X-3, 105	200.55	61.0	28.3	127.5
22X-4, 98	201.98	72.5	34.8	166.8
22X-5, 62	203.12	92.8	41.6	191.3
23X-1, 76	204.26	34.5	23.7	88.3
23X-2, 85	205.85	51.3	32.7	127.5
23X-CC, 52	208.26	54.8	33.9	196.2
24X-1, 85	213.95	34.5	22.2	107.9
24X-2, 85	215.45	35.4	24.8	127.5
24X-3, 85	216.95	76.0	46.7	166.8
24X-4, 85	218.45	82.2	47.0	186.4
24X-5, 85	219.95	73.4	45.6	171.7
25X-1, 35	223.15	44.2	22.6	78.5
25X-2, 37	224.67	83.1	35.3	152.1
25X-CC, 36	225.23	75.1	35.0	157.0
26X-1, 126	233.56	84.9	48.2	166.8
26X-2, 26	234.06	78.7	35.3	152.1
27X-1, 110	242.90	70.7	29.4	147.2
27X-2, 107	244.37	69.0	33.0	147.2
27X-3, 95	245.75	94.6	45.9	181.5
27X-4, 111	247.41	101.7	54.6	196.2
27X-5, 63	248.43	108.7	56.6	210.9
27X-6, 115	250.45	123.8	67.8	250.2
28X-1, 105	252.45	76.0	48.5	166.8
28X-2, 105	253.95	80.4	46.7	206.0
28X-3, 105	255.45	77.8	46.5	206.0
28X-4, 105	256.95	75.1	43.9	176.6
28X-5, 105	258.45	63.6	38.5	166.8
29X-1, 109	262.09	61.0	34.2	142.2
29X-2, 105	263.55	71.6	36.7	161.9
29X-3, 105	265.05	74.3	33.8	191.3
29X-4, 105	266.55	85.8	36.9	206.0
29X-5, 105	268.05	87.5	43.5	196.2
29X-6, 23	268.73	105.2	54.4	176.6
30X-1, 40	271.00	63.6	41.4	201.1
30X-2, 40	272.50	68.1	43.1	186.4
30X-3, 40	274.00	72.5	46.6	210.9
30X-4, 40	275.50	76.9	43.7	191.3
31X-1, 133	281.53	34.5	21.3	137.3
31X-2, 130	283.00	57.5	38.6	161.9
31X-3, 130	284.50	69.0	40.6	201.1
32X-1, 103	290.93	54.8	37.1	171.7
32X-2, 87	292.27	86.6	50.3	210.9
32X-3, 87	293.77	92.8	51.9	230.5
32X-4, 87	295.27	110.5	61.5	260.0
32X-5, 87	296.77	113.2	62.9	245.3
33X-1, 82	300.32	56.6	36.7	176.6
33X-2, 66	301.66	107.9	69.1	309.0
33X-3, 66	303.16	82.2	51.8	264.9
33X-4, 66	304.66	117.6	63.6	264.9
33X-5, 47	305.97	104.3	62.0	294.3

*Unconfined compressive strength (q_u) can be used to approximate undrained shear strength (S_u) by the relationship $q_u = 2S_u$.

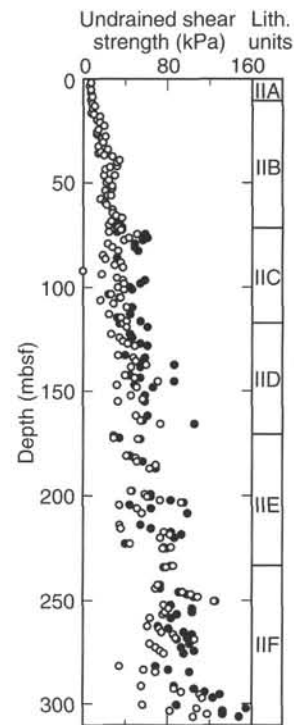


Figure 19. Undrained shear strength (open circles) and assumed undrained shear strength derived from unconfined compressive strength (solid circles) in Hole 938A.

IID. Seismic-facies Unit 4 records the activity of the Channel 5 and Yellow systems.

Seismic-facies Unit 5 (215–280 ms) is similar to seismic-facies Unit 4 and has medium-amplitude, continuous, divergent reflections; however, the Unit 5 reflections dip in the opposite direction toward the axis of Channel 6. The top of seismic-facies Unit 5 correlates with the contact between lithologic Subunits IID and IIE, which marks an abrupt downhole increase in silt laminae and sand beds. The character of the seismic reflections and the core lithology suggest that seismic-facies Unit 5 may represent overbank deposits that filled Channel 6 after it was abandoned.

Seismic-facies Unit 6 (280–500 ms) is characterized by low-amplitude, discontinuous irregular reflections, and the upper part correlates with lithologic Subunit IIF. These reflections are related to the silty clay with silt laminae associated with the overbank deposits of Channel-levee System 6.

IN-SITU TEMPERATURE MEASUREMENTS

Temperature gradients and heat flow were determined using two downhole measurements and the bottom-water (mud-line) temperature. Two ADARA measurements were made during Cores 938A-6H (55.1 mbsf) and -9H (83.6 mbsf) using instrument number 12. The mud-line temperature of 2.8°C measured from this instrument was used as the reference bottom-seawater temperature at Site 938. Successful measurements resulted in extrapolated equilibrium temperatures of 4.78°C at 55.1 mbsf, and 5.59°C at 83.6 mbsf.

Equilibrium temperatures, extrapolated from synthetic curves constructed to fit transient temperature data, are plotted as a function of depth (mbsf) in Figure 23. Using the ADARA mud-line temperature and the sub-bottom temperatures from the two ADARA mea-

Table 13. Electrical resistivity at Site 938.

Core, section, interval (cm)	Depth (mbsf)	Longitudinal resistivity (Ωm)	Transverse resistivity (Ωm)	Core, section, interval (cm)	Depth (mbsf)	Longitudinal resistivity (Ωm)	Transverse resistivity (Ωm)
155-938A-				15X-2, 90	134.00	0.368	0.361
1H-2, 40	1.90	0.283	0.246	15X-3, 90	135.36	0.379	0.370
1H-3, 60	3.60	0.243	0.237	15X-4, 90	136.86	0.384	0.384
1H-4, 80	5.30	0.256	0.255	15X-5, 90	138.36	0.372	0.372
1H-5, 105	7.05	0.278	0.265	16X-1, 82	142.02	0.379	0.361
2H-1, 104	8.64	0.298	0.276	16X-2, 82	143.52	0.371	0.371
2H-2, 84	9.94	0.299	0.270	16X-3, 82	145.02	0.388	0.381
2H-3, 105	11.65	0.289	0.273	16X-4, 77	146.47	0.357	0.373
2H-4, 89	12.99	0.292	0.272	16X-5, 77	147.97	0.377	0.364
2H-5, 73	14.33	0.321	0.299	17X-1, 105	151.85	0.382	0.383
2H-6, 111	16.21	0.313	0.289	17X-2, 105	153.35	0.375	0.372
2H-7, 58	17.18	0.324	0.297	17X-3, 107	154.87	0.405	0.385
3H-1, 91	18.01	0.340	0.293	18X-2, 10	161.48	0.389	0.377
3H-2, 91	19.51	0.293	0.283	18X-3, 60	163.48	0.392	0.400
3H-3, 89	20.99	0.288	0.283	18X-4, 93	165.31	0.408	0.412
3H-4, 105	22.65	0.278	0.271	19X-1, 71	170.81	0.392	0.400
3H-5, 102	24.12	0.298	0.270	19X-2, 74	172.34	0.351	0.324
3H-6, 82	25.42	0.321	0.312	19X-CC, 4	172.63	0.380	0.392
3H-7, 64	26.74	0.328	0.305	20X-1, 73	180.53	0.369	0.362
4H-2, 47	27.48	0.341	0.315	20X-2, 66	181.96	0.372	0.364
4H-3, 44	28.95	0.346	0.351	20X-3, 76	183.56	0.384	0.384
4H-4, 51	30.52	0.354	0.345	20X-4, 89	185.19	0.369	0.357
4H-5, 52	32.03	0.362	0.350	20X-5, 87	186.67	0.403	0.350
4H-6, 70	33.71	0.335	0.310	22X-1, 115	197.65	0.358	0.336
4H-7, 29	34.80	0.345	0.317	22X-2, 95	198.95	0.359	0.359
4H-7, 118	35.69	0.355	0.330	22X-3, 105	200.55	0.367	0.364
4H-8, 53	36.54	0.317	0.325	22X-4, 98	201.98	0.395	0.379
5H-1, 110	37.20	0.357	0.330	22X-5, 62	203.12	0.380	0.361
5H-2, 115	38.75	0.366	0.334	23X-1, 76	204.26	0.381	0.358
5H-3, 110	40.00	0.317	0.319	23X-2, 85	205.85	0.373	0.365
5H-4, 118	41.58	0.331	0.317	23X-CC, 52	208.26	0.384	0.384
5H-5, 51	42.41	0.255	0.294	24X-1, 85	213.95	0.381	0.374
5H-6, 25	43.65	0.314	0.292	24X-2, 85	215.45	0.355	0.343
5H-7, 113	46.03	0.324	0.311	24X-3, 85	216.95	0.384	0.401
6H-2, 59	46.43	0.285	0.279	24X-4, 85	218.45	0.392	0.364
6H-3, 127	48.61	0.349	0.314	24X-5, 85	219.95	0.381	0.361
6H-4, 90	49.74	0.347	0.333	25X-1, 35	223.15	0.370	0.345
6H-5, 93	51.27	0.338	0.317	25X-2, 37	223.74	0.381	0.386
6H-6, 88	52.72	0.347	0.324	25X-CC, 36	225.23	0.380	0.380
6H-7, 26	53.60	0.343	0.344	26X-1, 126	233.56	0.403	0.404
6H-8, 78	55.62	0.345	0.320	26X-2, 26	234.06	0.402	0.377
7H-2, 54	56.04	0.347	0.335	27X-1, 110	242.90	0.383	0.381
7H-3, 79	57.79	0.357	0.343	27X-2, 107	244.37	0.381	0.389
7H-4, 76	59.26	0.377	0.331	27X-3, 95	245.75	0.379	0.388
7H-5, 49	60.49	0.355	0.323	27X-4, 111	247.41	0.398	0.390
7H-7, 36	62.74	0.369	0.346	27X-5, 63	248.43	0.424	0.402
7H-8, 29	64.17	0.392	0.368	27X-6, 115	250.45	0.425	0.407
8H-1, 73	65.33	0.348	0.349	28X-1, 105	252.45	0.398	0.404
8H-2, 41	66.51	0.371	0.353	28X-2, 105	253.95	0.416	0.427
8H-3, 62	68.22	0.348	0.325	28X-3, 105	255.45	0.423	0.400
8H-4, 69	69.79	0.360	0.359	28X-4, 105	256.95	0.393	0.397
8H-5, 82	71.27	0.378	0.348	28X-5, 105	258.45	0.392	0.385
8H-6, 54	72.49	0.359	0.357	29X-1, 105	262.05	0.392	0.366
8H-7, 36	73.39	0.382	0.366	29X-2, 105	263.55	0.373	0.393
9H-1, 66	74.76	0.380	0.364	29X-3, 105	265.05	0.423	0.412
9H-2, 60	76.02	0.384	0.397	29X-4, 105	266.55	0.431	0.390
9H-3, 64	77.47	0.406	0.359	29X-5, 105	268.05	0.430	0.407
9H-5, 41	79.04	0.398	0.400	29X-6, 23	268.73	0.423	0.421
9H-6, 37	80.50	0.394	0.394	30X-1, 40	271.00	0.433	0.436
9H-7, 67	82.30	0.391	0.389	30X-2, 40	272.50	0.460	0.411
10X-1, 92	84.52	0.375	0.353	30X-3, 40	274.00	0.434	0.437
10X-3, 41	86.18	0.392	0.361	30X-4, 40	275.50	0.398	0.429
10X-4, 47	87.74	0.378	0.372	31X-1, 133	281.53	0.420	0.424
10X-5, 43	89.20	0.384	0.371	31X-2, 130	283.00	0.424	0.415
10X-6, 39	90.43	0.376	0.405	31X-3, 130	284.50	0.402	0.399
10X-7, 29	91.83	0.393	0.385	32X-1, 103	290.93	0.408	0.405
11X-1, 62	93.72	0.344	0.352	32X-2, 87	292.27	0.424	0.409
11X-2, 62	95.22	0.361	0.337	32X-3, 87	293.77	0.425	0.429
11X-3, 55	96.65	0.354	0.362	32X-4, 87	295.27	0.446	0.443
11X-4, 55	98.15	0.353	0.352	32X-5, 87	296.77	0.431	0.411
11X-5, 65	99.75	0.372	0.373	33X-1, 82	300.32	0.406	0.423
11X-6, 58	101.18	0.383	0.390	33X-2, 66	301.66	0.456	0.469
12X-1, 63	103.33	0.365	0.359	33X-3, 66	303.16	0.407	0.420
12X-2, 63	104.83	0.351	0.370	33X-4, 66	304.66	0.432	0.424
12X-3, 63	106.33	0.345	0.348	33X-5, 48	305.98	0.432	0.431
12X-4, 63	107.83	0.362	0.363				
12X-5, 63	109.33	0.388	0.360				
13X-1, 60	113.00	0.367	0.362				
13X-2, 60	114.50	0.408	0.417				
13X-3, 60	116.00	0.381	0.366				
13X-4, 60	117.50	0.384	0.375				
13X-5, 60	119.00	0.374	0.372				
14X-1, 60	122.60	0.371	0.367				
14X-2, 60	124.10	0.378	0.358				
14X-3, 60	125.60	0.360	0.354				
14X-4, 60	127.10	0.366	0.359				
14X-5, 35	128.35	0.390	0.369				
15X-1, 90	132.50	0.373	0.365				

surements downhole, the geothermal temperature gradient can be approximated by a linear mean of 33.6°C/km. We calculated heat flow by adopting the constant geothermal temperature gradient of 33.6°C/km and a linear increase in thermal conductivity, K, of $1.1 \pm 0.15 \text{ W/(m}\cdot\text{K)}$, which is an average of regression estimates at 80 mbsf. This results in a calculated heat flow of 36.98 mW/m².

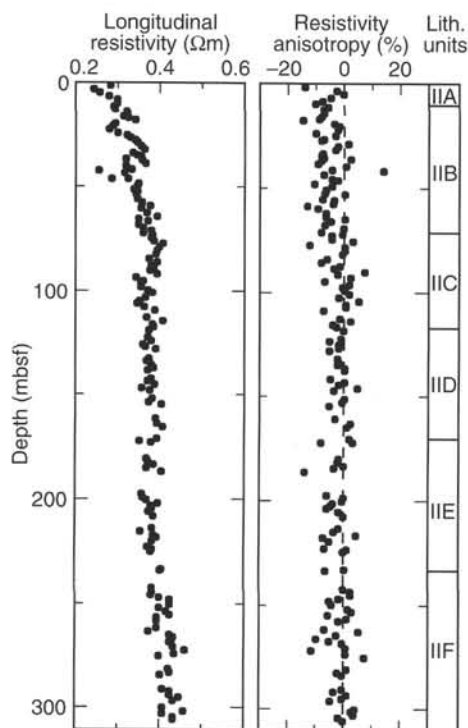


Figure 20. Longitudinal resistivity and electrical anisotropy in Hole 938A.

SYNTHESIS AND SIGNIFICANCE

Stratigraphic Synthesis

Surficial Foraminifer-Nannofossil Clay (Unit I)

Unit I (0–0.44 mbsf) is a bioturbated, Holocene foraminifer-nannofossil clay (Fig. 24), with 33% carbonate at 0.08 mbsf, similar to Unit I at other Leg 155 sites.

Bioturbated Mud Equivalent to the Amazon, Brown, Aqua, and Purple Channel-levee Systems (Subunit IIA and Upper Part of Subunit IIB)

Subunit IIA (0.44–10.55 mbsf) comprises bioturbated mud. The top 20 m of Subunit IIB (10.55–71.84 mbsf) is composed of bioturbated mud with silt laminae. These intervals are seismically correlated with the Amazon–Aqua and Purple Channel-levee systems. The active channels of these systems were, respectively, 40 and 55 km from this site.

Levee Crest of the Blue Channel-levee System (Lower Part of Subunit IIB and Subunit IIC)

The precise boundary between the Blue levee and the sediment equivalent to younger channel-levee systems is uncertain (but see Table 4 of Cisowski, this volume). The lower 30–40 m of Subunit IIB and all of Subunit IIC correspond to the Blue levee, and all but the lowest 15 m form a broadly fining-upward sequence. Subunit IIB is composed of mud with silt laminae and rare thin beds of silt and very fine sand. Subunit IIC (71.84–117.45 mbsf) consists of mud with numerous silt laminae and beds of silt and very fine sand. Burrow motes are common and many disrupt silt laminae. Sand beds are up to 9 cm thick.

Bioturbated Mud Equivalent to the Yellow Channel-levee System (Subunit IID)

Subunit IID (117.45–170.53) is mud with rare silt laminae and common bioturbational mottling. Carbonate content averages 3.6% and reaches 18.9% in a 2-cm-thick light-colored interval that may be a clast. A few loosely cemented diagenetic nodules of siderite were observed. This interval corresponds to active sedimentation of the Yellow Channel-levee System that was cored 10 km to the east at Site 937.

Abandoned-channel-fill Turbidites Equivalent to the Yellow and/or Channel 5 System (Subunit IIE)

Subunit IIE (170.53–233.73 mbsf) consists of mud with abundant laminae and thin beds of silt and very fine sand. Recovery was only 50% in this interval, suggesting that more sand may have been present than was recovered. Subunit IIE is correlated seismically with the Yellow and/or Channel 5 Channel-levee system. The seismic-reflection profile suggests that these deposits have partially filled the abandoned Channel 6.

Levee Crest of the Channel 6 System (Subunit IIF)

The Channel 6 levee, at its crest, is about 200 m thick. Subunit IIF (233.73–306.35 mbsf), which sampled the upper part of this levee, consists of mud with laminae and thin beds of silt and very fine sand, but in less abundance than in Subunit IIE. The average carbonate content exceeds 3%, compared with <2.5% in the overlying subunit.

Implications

Nannofossils are abundant in Unit I but are rare and poorly preserved in Unit II. Foraminifer abundances are generally high in Unit I, moderate in Subunits IIA, part of IIC and IID, and low elsewhere. At 149 mbsf, *P. obliquiloculata* reappears, indicating an age >40 ka, and is common in deeper sediment. The absence of *G. menardii* and *G. tumida* at the base of the hole indicates an age <85 ka. These biostratigraphic datums are consistent with those at Sites 931 and 932.

An apparent paleomagnetic excursion was tentatively identified at 145 mbsf within an XCB core. This event has a character similar to the Lake Mungo Excursion (30 ka) that was identified at a similar seismostratigraphic level at Sites 930 and 933. It occurs only 4 m above the Y_p obliq. datum, which is about 10 k.y. older. The interval between the two datums consists of bioturbated mud with a relatively high carbonate content: it is possible that this represents a slowly deposited interval.

Oscillations in the paleomagnetic-declination records at two intervals in Hole 938A are interpreted as secular variation. Between 15 and 45 mbsf, five cycles are present within the upper part of the Blue levee system. These can be correlated with cycles of similar character within the Blue interval in Holes 937B (24.0–27.5 mbsf) and 930C (64.5–72.5 mbsf). Another 16 cycles of declination are found between 70 and 78 mbsf in Hole 938A.

The proportion of illite (and mica) to other clay minerals is highest in the interval from 20 to 40 mbsf, corresponding to hemipelagic sediment equivalent to the Amazon, Aqua, and Purple seismic stratigraphic intervals. A similar pattern is seen at Site 936 over the same seismic stratigraphic units, but at that site the interval is in levee facies. This suggests that the trend reflects changes in the mineralogy of sediment supplied to the fan, rather than being a consequence of analyzing samples of different grain sizes.

Several lines of evidence suggest that the bioturbated muds accumulated more slowly than the levee crest sequences. This evidence includes changes in the trend of the water-content downhole profile that correspond approximately to the upper boundaries of Subunits

IID and IIF. Abyssal benthic foraminifers are found in finer grained intervals of Subunits IIB and IIC, suggesting periods of lower sedimentation rate: bathyal benthic foraminifers in Subunits IID and IIE are associated with iron-stained foraminifers, wood, and mica, and indicate that much of the biogenic component is re-sedimented.

The channel-fill deposits of Unit IIE are an interesting contrast with the medium to coarse sand fill of the active channel sediment sampled at Site 934. Only fine sand is present in Unit IIE: a grain size that is common in overbank levee deposits. Either the seismic interpretation of a channel is incorrect, or the sediment filling the channel were derived from spillover of turbidity currents from a different active channel.

REFERENCES*

Curry, W.B., Shackleton, N.J., Richter, C., et al., in press. *Proc. ODP, Init. Repts.*, 154: College Station, TX (Ocean Drilling Program).

Damuth, J.E., 1977. Late Quaternary sedimentation in the western equatorial Atlantic. *Geol. Soc. Am. Bull.*, 88:695-710.

Damuth, J.E., Flood, R.D., Kowsmann, R.O., Belderson, R.H., and Gorini, M.A., 1988. Anatomy and growth pattern of Amazon deep-sea fan as revealed by long-range side-scan sonar (GLORIA) and high-resolution seismic studies. *AAPG Bull.*, 72:885-11.

Damuth, J.E., Kowsmann, R.O., Flood, R.D., Belderson, R.H., and Gorini, M.A., 1983. Age relationships of distributary channels on Amazon deep-sea fan: implications for fan growth pattern. *Geology*, 11:470-473.

Manley, P.L., and Flood, R.D., 1988. Cyclic sediment deposition within Amazon deep-sea fan. *AAPG Bull.*, 72:912-925.

*Abbreviations for names of organizations and publications in ODP reference lists follow the style given in *Chemical Abstracts Service Source Index* (published by American Chemical Society).

Ms 155IR-114

NOTE: For all sites drilled, core-description forms ("barrel sheets") and core photographs can be found in Section 4, beginning on page 703. Forms containing smear-slide data can be found in Section 5, beginning on page 1199. GRAPE, index property, magnetic susceptibility, and natural gamma data are presented on CD-ROM (back pocket).

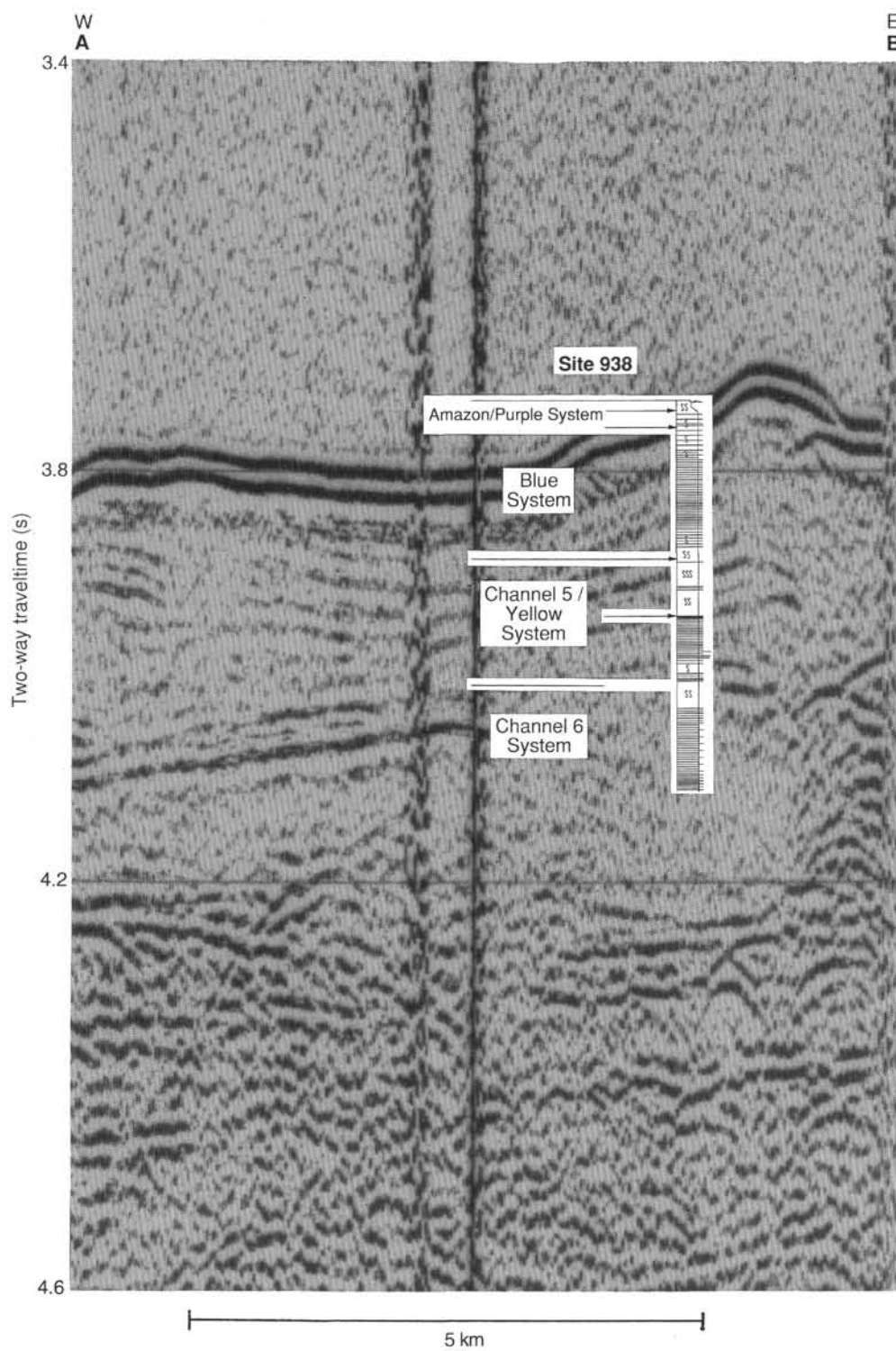


Figure 21. Seismic-reflection profile showing Site 938 with the corresponding lithostratigraphic section, prominent reflections, and seismic units. Location given in Figure 1, "Site 937" chapter, this volume. Arrows point to prominent reflections.

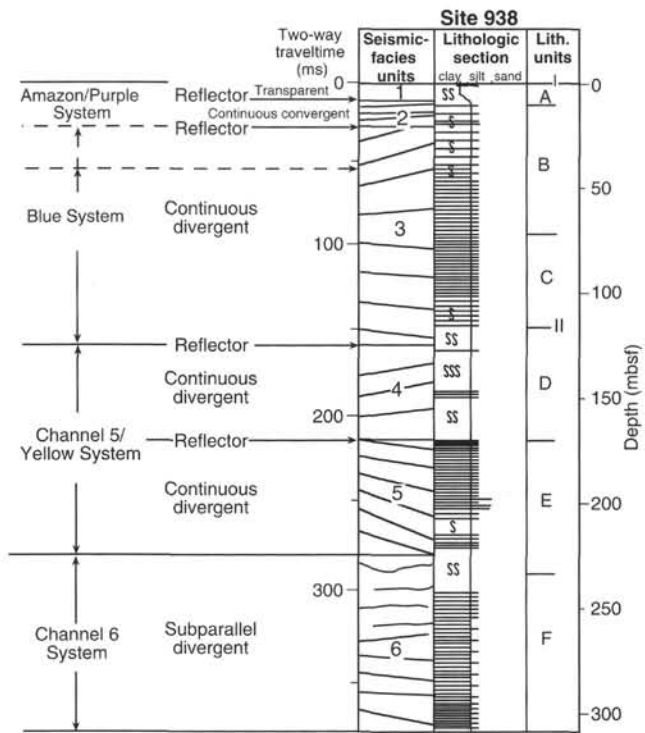


Figure 22. Correlation of lithostratigraphic observations with seismic-facies units and prominent reflections at Site 938.

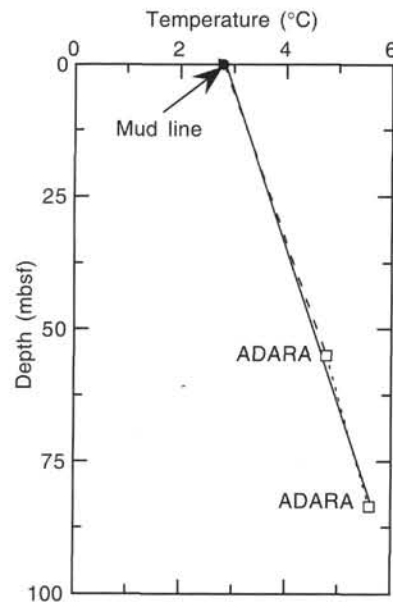


Figure 23. Estimated equilibrium temperatures in Hole 938A. A linear curve fit (solid line) through the data suggests that reliable equilibrium temperatures were acquired that indicate a geothermal gradient of 33.6°C/km. A geothermal temperature gradient of 35.8°C/km is calculated (dashed line) by using the ADARA mud-line temperature and the one ADARA measurement at 55.1 mbsf. A geothermal temperature gradient of 28.4°C/km is calculated (dotted line) by using both ADARA measurements.

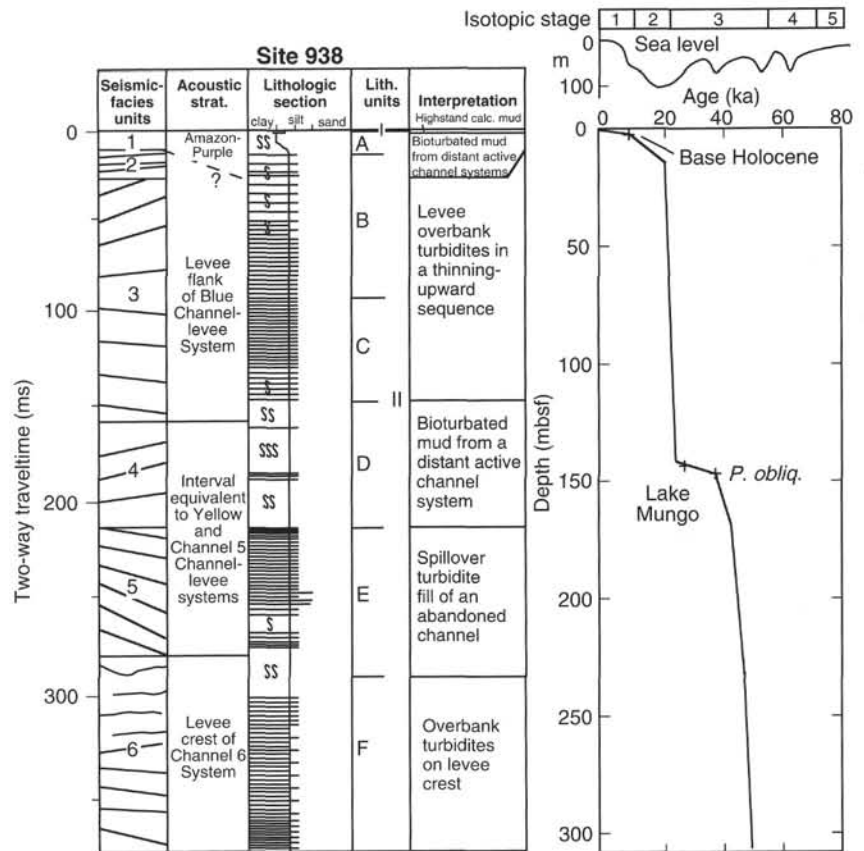


Figure 24. Summary of Site 938 showing (left to right) seismic-facies units, acoustic stratigraphy, schematic lithologic column, lithologic units, log stratigraphic units, interpreted sediment facies, chronological picks, and interpreted age-depth curve (+ = datums; variations in slope between these points are interpreted, based on dated intervals of similar facies at other sites).